Master's thesis
Master's program in Atmospheric Sciences
Biosphere-atmosphere interactions

Non-growing season CO_2 and energy fluxes from a subarctic ecosystem

Milla Karlsson

November 25, 2025

Supervisor(s): PhD. Anna-Maria Virkkala,
Prof. Timo Vesala,
MSc. Asta Laasonen

Examiner(s): Prof. Ivan Mammarella
Prof. Timo Vesala

University of Helsinki
Faculty of Science
PL 64 (Gustaf Hällströmin katu 2a)
00014 University of Helsinki

HELSINGIN YLIOPISTO — HELSINGFORS UNIVERSITET — UNIVERSITY OF HELSINKI

Tiedekunta — Fakultet — Faculty	Koulutusohjelma — Utbildningsprogram — Degree programme
Faculty of Science	Master's program in Atmospheric Sciences Biosphere-atmosphere interactions

Tekijä — Författare — Author

Milla Karlsson

Työn nimi — Arbetets titel — Title

Non-growing season CO_2 and energy fluxes from a subarctic ecosystem

Työn laji — Arbetets art — Level	Aika — Datum — Month and year	Sivumäärä — Sidantal — Number of pages
Master's thesis	November 25, 2025	38

Tiivistelmä — Referat — Abstract

Arctic soils store vast amounts of carbon, some of which will be potentially released due to climate change induced warming. Since Arctic areas are particularly vulnerable to climate change, it is urgent to understand how warming will shape the carbon exchange in high-latitude ecosystems. While the wintertime carbon exchange in the Arctic has been historically assumed to be negligible, recent evidence suggests that it may significantly affect the annual carbon balance. This study analyzes the eddy covariance (EC) CO_2 flux data from Kilpisjärvi subarctic site during August–January in 2024–2025. The evolution of CO_2 flux and radiation components during the measurement period is presented, and the significance of different environmental factors affecting CO_2 flux is analyzed separately for autumn (August–October) and winter (November–January) periods. Furthermore, the energy balance (EB) of the site is assessed. The EC data was gapfilled using random forest and the flux was partitioned into gross primary production and ecosystem respiration using the nighttime approach.

The diurnal CO_2 flux has a distinct pattern during August and September, when photosynthesis is active during the day. The diurnal cycle fades rapidly as the months progress, and respiration rate exceeds photosynthesis rate in October. The CO_2 flux is close to zero, but remains positive throughout the winter, indicating that respiration takes place in the soil. The release of CO_2 during winter causes a cumulative flux of 55.4 $\mathrm{gC\,m^{-2}}$ during the whole measurement period. A permanent snowpack forms halfway through November, allowing the soil to maintain a relatively warm temperature during the winter (mean -0.6°C). During winter, soil temperature is the only driver of CO_2 flux. In turn, photosynthetically active radiation and relative humidity are the most significant drivers for CO_2 flux during autumn. The energy balance closure (EBC) is sufficiently high during August (91%), September (86%) and November (90%), but lower for other months. Sensible heat flux largely counterbalances the negative net radiation during winter, whereas latent and ground heat fluxes are negligible. The results indicate that Kilpisjärvi is a carbon source during the winter since snowpack allows the soil to maintain a fairly warm temperature which supports microbial respiration. The results stress the need for around-year flux measurements to determine the future of the Arctic carbon budget.

Avainsanat — Nyckelord — Keywords

Eddy covariance, Subarctic, CO_2 flux, Energy balance, Carbon exchange, Kilpisjärvi

Säilytyspaikka — Förvaringsställe — Where deposited

The Helsinki University Library

Muita tietoja — Övriga uppgifter — Additional information

ChatGPT was used as support in plotting figures and building the code used for analysis.

Contents

1. Introduction

Warming of the Arctic (north of 66.5°N) has been 3.8 times as strong as the global average during the years 1979–2021 (Rantanen et al., 2022). This phenomenon, known as Arctic amplification, is strongest in late autumn and weakest during the growing season (Rantanen et al., 2022). The northern circumpolar permafrost zone stores approximately 1700 Pg of organic carbon in the soil, some of which is expected to be released progressively due to climate change (Schuur et al., 2013). Changes in climatic and local weather conditions, especially temperature and snow conditions, permafrost thaw and vegetation shifts profoundly affect the release of soil carbon in the Arctic. Furthermore, belowground processes are critical controllers of CO_2 emissions outside the growing season, as well as factors controlling oxygen availability and carbon substrates (Arndt et al., 2023). Global warming and the following tundra greening is projected to increase both primary production and heterotrophic respiration in the Arctic (McGuire et al., 2009; Shaver et al., 1992). The relative magnitude of these changes will determine whether the ecosystem functions as a carbon sink or a source in the future.

While historically the Arctic has been considered a net sink of carbon due to overlooked wintertime activity, recent studies indicate that the area has transformed into a carbon source owing to rising air temperatures. For instance, Grogan and Jonasson (2006) and Oechel et al. (2014) found wintertime CO_2 production in a subarctic tundra site to significantly affect the annual carbon balance of the ecosystem, mainly due to the long duration of winter. Wintertime CO_2 fluxes vary significantly between different tundra sites, and are estimated to be 7% of total annual soil respiration in shrub-dominated sites (Hobbie et al., 2000). Moreover, Commane et al. (2017) estimated regional CO_2 fluxes in Alaska by combining aircraft and eddy covariance measurements, remote sensing and meteorological drivers. They observed that tundra ecosystems were a net source of CO_2 annually due to increase in early winter respiration, which correlates with rising air temperatures. They claim that respiration has increased 73% since 1975 at North Slope of Alaska. Generally, wintertime CO_2 fluxes in cold environments have been found to be positive although their exact magnitude is still uncertain (Hobbie et al., 2000).

The carbon flux data at Arctic sites during winter is limited compared to the data collected during the growing season (Arndt et al., 2023; Oechel et al., 2014), due to difficult

field conditions, extreme cold and isolation of such places. Thus, there are large uncertainties in how the carbon fluxes will change with respect to climate change and what is the relative magnitude of wintertime carbon fluxes to annual carbon balance. Under current climatic conditions, Natali et al. (2019) estimate a yearly loss of 1.662 Tg of carbon from the permafrost region during the winter season ranging from October to April. They note that the current rate may be offsetting the CO_2 uptake by vegetation during the growing season. Year-round flux measurements are needed since wintertime phenomena, for instance snow accumulation, affect the heat and scalar fluxes during the followig summer as well (Oechel et al., 2014). In Arctic areas, the most dynamic environmental events happen during spring and autumn, often referred to as the shoulder seasons. However, according to Weller and Holmgren (1974), the wintertime 'characterizes the true nature of the Arctic tundra as part of the polar heat sink', as the polar night substantially alters the energy balance (EB). The radiation conditions affect the CO_2 exchange through variables such as moisture, temperature, snow cover and photosynthetically active radiation (PAR).

Furthermore, it remains uncertain how different environmental factors, such as snow cover, vegetation composition, temperature and radiation conditions affect wintertime carbon exchange in high-latitude ecosystems. The relationship between CO_2 flux and several environmental variables varies significantly by season (López-Blanco et al., 2017; Oechel et al., 2014). Thus, it is crucial to conduct flux measurements during all seasons to obtain reliable predictions of the future of Arctic ecosystems. Carbon loss or gain in the Arctic region have the potential to induce feedbacks on the global atmospheric concentration of CO_2 (Shaver et al., 1992). Therefore, climate change directly affects the functioning of Arctic ecosystems, but it may also induce positive feedbacks between global climate and ecosystems (Oechel et al., 2014), and climate change induced changes in the Arctic can be seen as warnings of larger, but slower global responses (Shaver et al., 1992).

This study aims to

1) Provide an insight into the net carbon exchange in Kilpisjärvi subarctic station using eddy-covariance data collected during the non-growing season (August–January in this study) in 2024–2025. The evolution of diurnal cycle of CO_2 will be presented and the relative contributions of ecosystem respiration and gross primary production will be investigated, as well as the cumulative CO_2 flux throughout the measurement period.

2) Determine the contribution of different environmental variables controlling carbon exchange in a subarctic shrubland during the non-growing season.

3) Assess the radiation balance of the site focusing on its seasonal transition and evolution from late autumn through to the polar night. In addition, the energy balance closure (EBC) will be briefly covered.

2. Theory and background

This chapter briefly introduces the theory behind the eddy covariance method. Moreover, CO_2 dynamics at high latitudes are discussed, and the effects of environmental factors characteristic to Arctic regions to CO_2 exchange are reviewed. Finally, the theory of EB is described.

2.1 Turbulence in the planetary boundary layer

The planetary boundary layer is defined by Stull (1988) as the lowest part of the troposphere that is directly influenced by the presence of the Earth's surface and responds rapidly to surface forcings. Surface forcings, such as frictional drag, and solar heating produce turbulence, which is the main vertical transport mechanism of energy and mass in the boundary layer. Turbulence is characterized by different-sized eddies, which transform energy from larger to smaller scales, eventually resulting in dissipation (Tennekes & Lumley, 1972). The bottom of the boundary layer is called the surface layer, where turbulent fluxes vary very little with height and therefore can be assumed to be approximately constant (Aubinet et al., 2012). An inversion layer, which is mostly stable and where turbulence is weaker, separates the boundary layer from the free atmosphere.

The height of the boundary layer over land surfaces varies diurnally, and is mainly driven by radiative warming and cooling (Kaimal & Finnigan, 1994). After sunrise, solar radiation heats up the surface, and heat transfer from the surface warms the above-lying air, creating a highly turbulent convective layer, which grows to full extent by mid-afternoon. The surface layer is well-mixed and unstable during the day, and extends to 20–50 m height. The mixed layer dissipates as the surface thermal forcing weakens, causing the ground to cool quickly, and an inversion layer to form as the cool air mixes upwards. A stable boundary layer develops near the ground, with a neutrally stratified residual layer above it. The stable boundary layer is characterized by strong wind shear and small-scale eddies (Kaimal & Finnigan, 1994), and its height is generally a few meters (Foken & Nappo, 2008). In winter, especially in high latitudes, there is very little energy transport to the surface due to lack of solar radiation, which causes a strong stratification to the boundary layer (Foken & Nappo, 2008).

2.2 Overview of eddy covariance technique

Eddy covariance is a widely utilized non-destructive and non-invasive method used to measure energy and scalar fluxes on ecosystem scale. It is based on assumptions that over a flat and horizontally homogeneous surface, the net transport of heat, mass, and momentum between the surface and the atmosphere is one dimensional, and turbulence is statistically stationary. Thus, the vertical flux density of a desired component can be calculated by the covariances between the representative component and turbulent fluctuations of vertical wind (Montgomery, 1948; Obukhov, 1951; Swinbank, 1951). The assumption is valid in the surface layer.

According to Reynolds (1895) the time series of the variables associated with turbulent motions can be partitioned into mean and fluctuating parts. For instance the time series of an arbitrary scalar ψ can be described with

$$\Psi = \overline{\Psi} + \psi' \tag{2.1}$$

where $\overline{\Psi}$ is the time-average

$$\overline{\Psi} = \frac{1}{T}\int_{t}^{t+T} \Psi(t)dt, \tag{2.2}$$

T is the total time interval and $\psi^{'}$ is its time-dependent, fluctuating component. Reynold's averaging allows for the isolation of large-scale variations from turbulent ones, and together with Bouissinesq-approximation [†] simplifies the equations of turbulent motions.

The conservation equation for a scalar (ψ) in the atmosphere is written in (Aubinet et al., 2012) as

$$\frac{\partial \rho_d \psi}{\partial t} + \vec{\nabla}(\vec{u}\rho_d\psi) + K_\psi \Delta(\rho_d\psi) = S_\psi \tag{2.3}$$

where $\vec{u}$ is the wind velocity and ρ_d is dry air density. The first term on the left-hand side represents the rate of change of the scalar, which is affected by the following terms: atmospheric transport and molecular diffusion, respectively. The term on the right-hand side is the production/absorption of the scalar by a source/sink. Applying Reynold's averaging to the scalar conservation equation, integrating it in a control volume and assuming horizontal homogeneity and negligible vertical advection, yields the equation governing the basis of the eddy covariance method. It is presented by Aubinet et al. (2012) as

$$\int_0^{h_m} \overline{\rho_d}\overline{\frac{\partial \psi_s}{\partial t}}dz + \overline{\rho_d}\overline{w'\psi_s'}|_{h_m} = F_s \tag{2.4}$$

[†]Bouissinesq-approximation states that horizontal density variations are negligible.

where the first term on the left-hand side represents the storage term of the scalar χ_s, the second term represents the vertical turbulent flow at the top of the control volume, and the term on the right-hand side is the respective flux of the scalar. The above equation represents the flux well under well-mixed, unstable conditions when turbulence is fully developed. However, in a stable atmosphere where turbulent transport is weak, e.g. during nighttime, the eddy covariance method underestimates all turbulent fluxes including the CO_2 flux (Aubinet et al., 2012). Friction velocity is a measure of shear stress expressed as velocity and thus useful in determining turbulence conditions. When the x-axis points in the direction of surface stress, friction velocity is defined in Stull (1988) as

$$u_*^2 = |\overline{u'w'}| \tag{2.5}$$

where $\overline{u'w'}$ is the covariance of vertical and horizontal wind components. At nights, the CO_2 flux is sensitive to friction velocity, even though there should not be a significant relation between the two. Typically, at sufficiently small friction velocity values the flux values tend to decrease (Aubinet et al., 2012). According to Aubinet et al. (2012), the night-flux error appears at all sites on nights with low turbulence. Thus, a filtering procedure should be applied to remove data points at times when turbulence conditions are poor.

Similarly, the turbulent energy fluxes can be calculated with the covariance between vertical wind fluctuations and a representative scalar:

$$SH = \rho_d c_p \overline{w'\theta'} \tag{2.6}$$

and

$$LE = \rho_d L_v \overline{w'q'} \tag{2.7}$$

where SH is the sensible heat flux, θ' is the fluctuating component of potential temperature (regular air temperature was used in this analysis), LE is the latent heat flux, L_v is the latent heat of vaporization of water and q' is the fluctuating part of specific humidity. Turbulent heat fluxes are discussed in more detail in section 2.6.

2.3 CO_2 exchange processes and dynamics

The net ecosystem exchange (NEE) describes the difference between uptake of CO_2 through photosynthesis and release of CO_2 through respiration. NEE can be partitioned into gross primary production (GPP), describing the total amount of organic matter produced via photosynthesis, and ecosystem respiration (ER), which is the total amount of CO_2 produced by autotrophic and heterotrophic respiration. Photosynthesis and respiration are the main factors controlling CO_2 exchange in terrestrial ecosystems. Over the

non-growing season photosynthetic activity ceases due to lack of sunlight and decreasing temperatures, and respiration causes emissions of CO_2 into the atmosphere. CO_2 flux is defined negative when the rate of CO_2 taken up by plants is larger than ecosystem respiration rate. Similarly, when ecosystem respiration rate exceeds photosynthesis rate, CO_2 flux is defined positive.

CO_2 flux generally has a distinct diurnal cycle; the flux is positive during the night and negative during the day when photosynthesis takes place. However, during the Arctic winter months, when sunlight is lacking, this diurnal pattern breaks as photosynthetic activity ceases. Winter climate conditions, especially soil temperature and snowfall, as well as vegetation type can significantly affect regional patterns of CO_2 release (Grogan & Jonasson, 2006), but plenty of other factors play a role as well. Webb et al. (2016) found that soil temperature (especially at 10 cm), day of the season, atmospheric pressure, air temperature and the interactions between the last two were significantly related to CO_2 flux. Air temperature and pressure affect gas diffusion from the soil to the atmosphere, which is especially important during the autumn, when gases trapped in the soil during the growing season are released, potentially causing an additional flow of CO_2 to the atmosphere (Arndt et al., 2023). In contrast, Oechel et al. (2014) found that net radiation was a significant predictor of CO_2 fluxes in all seasons, while soil temperature was only important during summer and autumn. Furthermore, relative humidity (RH) affects stomata opening and closing, and therefore also the CO_2 flux. Lower RH indicates drier air and, if sufficiently large, may cause plants to close their stomata in order to avoid drought.

2.3.1 Effects of soil and air temperature

In shrub-dominated ecosystems of northern latitudes, soil temperature is a significant predictor of NEE (Cahoon et al., 2012; Mikan et al., 2002). This is mainly due to the decrease in the rate of microbial decomposition caused by cold temperatures, although soil moisture and substrate quality also play an important role (Hobbie et al., 2000). Nonetheless, Mikan et al. (2002) found that microbial respiration can continue even at soil temperatures of -10°C, and Grogan and Jonasson (2006) measured substantial CO_2 effluxes from a subarctic heath-tundra site in the coldest phase of winter. They found significant correlation between soil temperature and CO_2 release in wintertime. At a regional scale, decomposition is controlled primarily by vegetation composition, surface topography and temperature (Hobbie et al., 2000), but snow depth may have a significant effect on respiration rates as well (Grogan & Jonasson, 2006). The accumulation of snow insulates the soil, allowing warmer temperatures and continuous microbial activity potentially throughout the winter (Hobbie et al., 2000). Part of the CO_2 produced by

respiration during winter accumulates within the soil and the snow layer (Grogan & Jonasson, 2006) and is released as the snow melts. Furthermore, decomposition has been found to be more rapid in upland sites with oxic soil conditions (Hobbie et al., 2000), indicating that soil water content may affect CO_2 fluxes as well. Additionally, soil mixing by freeze-thaw processes especially during spring and autumn — a phenomenon known as cryoturbation — affects decomposition rates (Hobbie et al., 2000).

Temperature influences a wide variety of ecosystem processes, so differences between short- and long-term responses to climate change are expected (Elmendorf et al., 2012). Mikan et al. (2002) underscore the potential of warming to stimulate microbial activity during winter and thus increase CO_2 emissions from tundra soils. Increased air temperature or snow accumulation likely increase the rate of biogeochemical processes at sites where the snow depth typically stays below one meter. The effect would be most enhanced in areas with moderate vegetation stature, such as shrub tundra, which would be trapped below the snowpack, where temperature stays higher than in the surrounding air (Grogan & Jonasson, 2006).

2.3.2 Effects of vegetation

The response of tundra vegetation to climate warming is expected to vary both spatially and temporally, and there is much uncertainty about when and where vegetation changes will take place (Elmendorf et al., 2012). Temperature has been limiting shrub growth in the Arctic. Thus, it is likely that climate change will increase the relative abundance of shrub species in Arctic areas (Myers-Smith et al., 2011). The phenomena is known as shrub enroachment and it has already been witnessed in several areas across the Arctic (Myers-Smith et al., 2011). Warming generally increases litter accumulation, mean canopy height and the abundance of tall shrubs in relatively warm and moist sites (Elmendorf et al., 2012). Increasing microbial activity and litter decomposition due to warmer temperatures further favor shrub growth. Shrub enroachment will cause an increase in summertime sensible heat flux, soil shading and litter production, and a decrease in wintertime albedo (Elmendorf et al., 2012). In winter, shrub cover may localize snow accumulation, allowing warmer soil temperatures on areas with more snow. Similarly, leaf area expansion during summer shades the ground, allowing warmer soil temperatures (Myers-Smith et al., 2011). Shrub enroachment alters nutrient exchange as well, but it is not yet certain how and in which direction (Myers-Smith et al., 2011). Arctic areas are generally strongly nutrient-limited, and most carbon and nutrients reside in soil organic matter, which has slow turnover rates (Shaver et al., 1992). Increasing temperature will not strongly increase net primary production unless nitrogen mineralization — conversion of organic nitrogen into inorganic form — increases as well, since carbon to nitrogen (C:N)

ratio in plants limits the carbon accumulation (Shaver et al., 1992).

Variation of plant species composition plays a role in CO_2 exchange as well. *Empetrum*, a genus of evergreen dwarf shrubs, are somewhat drought sensitive. In subarctic areas, their presence depends on snow cover during winter, which allows protection against freezing and winter drought (Tybirk et al., 2000). The leaves and litter of *Empetrum* have high phenolic content, resulting in slow decomposition (Tybirk et al., 2000). Increased temperature and nitrogen availability may in turn favor *Betula nana* (Myers-Smith et al., 2011). According to (McLaren et al., 2017), *Betula* have a relatively high aboveground decomposition rate, but the rate decreases when mixed with other species. They suggest that the negative mixing effects constrain the increase in decomposition rate until *Betula* becomes dominant. If this happens, the increase in decomposition implies more rapid carbon turnover rates in the Arctic, and perhaps further increase in shrub abundance.

2.4 CO_2 flux partitioning

Flux partitioning is done to analyze the variation of NEE with respect to photosynthesis and respiration (Lasslop et al., 2012). NEE is partitioned into GPP and ER according to

$$NEE = ER - GPP. \tag{2.8}$$

Partitioning allows the investigation of the drivers of photosynthesis and respiration as separate processes. It is typically done according to the following assumptions:

1) Temperature is the driving force of ecosystem respiration.
2) Photosynthesis ceases at night.

Therefore, the nighttime CO_2 flux has a distinct relationship with respect to temperature, although moisture can affect the relationship between NEE and temperature by limiting respiration or changing the transport processes of heat and CO_2 (Lasslop et al., 2012). In a subarctic shrubland outside the growing season, soil respiration is assumed to be the dominant part of ecosystem respiration; it induces the most significant effect on respiration. The top soil layer is usually the largest source of soil respiration and the correlation between nighttime NEE and temperature on average decreases with increasing observation depth (Lasslop et al., 2012). The partitioning method is covered more thoroughly in section 3.2.2.

2.5 Storage fluxes

The storage fluxes are explained according to the definition presented in Montagnani et al. (2018). The storage term represents the temporal variation of the dry molar fraction of a

gas or another scalar in a control volume representative of the turbulent flux. Friction velocity, which quantifies the amount of turbulence, influences the storage terms. Moreover, variations in the storage term of CO_2 can be due to photosynthesis or respiration, and variations in the storage terms of turbulent heat fluxes can be caused, for example, by the formation of dew and fog. Including the storage fluxes not only increases the reliability of CO_2 flux measurements, but it might improve the EBC as well. Nevertheless, the storage terms are usually small on areas with low vegetation where measurement height is low as well. The equation for storage fluxes is presented by (Montagnani et al., 2018) as:

$$J_c = \int_0^h \overline{\rho_d} \frac{\delta c}{\delta t} \delta x_3 \approx \sum_{i=1}^{N} \overline{\rho_{d_i}} (\frac{\Delta c}{\Delta t})_i \Delta z_i \tag{2.9}$$

where ρ_d is the dry air density, Δt is the time interval, Δc is the concentration gradient and Δz is the difference between measurement heights.

2.6 Energy balance

The Earth's surface works as an important area for energy transfer processes. Incoming shortwave radiation is absorbed ($SW \downarrow$) and reflected ($SW \uparrow$) by the surface. Furthermore, the surface absorbs ($LW \downarrow$) and emits ($LW \uparrow$) the incoming longwave radiation originating from clouds, particles and gases in the atmosphere. Net radiation is the sum of the above-mentioned components, and can thus be positive or negative. It is defined by Foken and Nappo (2008) as

$$R_n = SW \uparrow + SW \downarrow + LW \uparrow + LW \downarrow \tag{2.10}$$

Net radiation is positive during sunlight hours, when the incoming radiation is much larger than the outgoing components. Snow is often present in the Arctic during winter, and due to its high albedo, nearly all shortwave radiation is reflected back into the atmosphere. At nights and during the polar night in high latitudes, emissions of shortwave radiation cease, and the net radiation is controlled only by longwave radiation terms. Due to snow's high emissivity of thermal radiation, longwave radiation is emitted by the ground into the atmosphere more than is gained from the atmosphere, resulting in negative net radiation. Available energy affects both photosynthesis and respiration rates (Oechel et al., 2014), which is why EB is important to consider when analyzing CO_2 fluxes.

The surplus of energy at the Earth's surface is transported back into atmosphere by turbulent latent and sensible heat fluxes. Moreover, energy is transported into or out of the ground by the ground heat flux. EB describes the equilibrium between incoming and outgoing energy. It is derived from the first law of thermodynamics, and insists that turbulent heat fluxes must be equivalent to all other energy sinks and sources (Wilson

et al., 2002). The energy balance can be formulated as

$$LE + SH = R_n - G - S \tag{2.11}$$

where LE and SH are latent and sensible heat fluxes, respectively, R_n is the net radiation, G is the ground heat flux and S is the rate of change of heat storage (eg. in vegetation, air and soil). S is not used in following equations since the air storages of LE and SH is included in their calculations, and the vegetation and soil storages are assumed negligible.

The ground heat flux describes heat conductance between the surface and the underlying soil. In this study, effects of snow and ground vegetation to heat transport are neglected and soil heat flux is assumed representative of G. It is defined positive when heat is transported from the ground surface into the deeper soil layers. It is driven by temperature gradients, and follows the pattern of net radiation with a certain time lag. While soil structure and moisture significantly affect G, the fraction of G to R_n is controlled by leaf-area index (LAI) and stem area as well, which influence surface shading and albedo (Eugster et al., 2000). Thus, the significance of G depends on the ecosystem. Generally it is relatively small compared to other heat fluxes, but in certain Arctic areas, it has been shown to be significant during winter (Langer et al., 2011).

Turbulent heat fluxes are defined positive when heat is transported away from the surface into the atmosphere. LE is related to phase changes of water; evaporation takes up energy, while condensation releases it. LE is positive when evapotranspiration takes place, which in turn is controlled by LAI, RH and stomatal conductance (Eugster et al., 2000). It is expected to be small in cold and dry regions with limited vegetation cover, although evaporation and sublimation occur during snow cover (Kasurinen et al., 2014), as well as during freeze-thaw processes in the soil (Weller & Holmgren, 1974). SH describes heat exchange between air and the ground by conduction and without phase changes. It is driven by temperature gradients, surface roughness, and indirectly net radiation. Therefore SH directly feedbacks to air temperature and thus also to the height of the boundary layer (Eugster et al., 2000). When SH is positive, heat flows from the ground to the air, causing air temperature to rise and the surface to cool. SH is generally positive during the day when incoming solar radiation causes the ground to warm more than the above air. During the Arctic winter, when no sunlight is available, SH is expected to be negative, since the ground cools by longwave emissions.

A general problem governing all eddy-covariance sites is that the EB is not completely closed (Wilson et al., 2002). Often, the turbulent heat fluxes are underestimated and thus are not sufficient to balance the available energy. The reasons for non-closure of the EB might be due to instrumental and data processing errors, additional neglected terms of the EB equation (e.g. horizontal advection and flux divergence) and submesoscale transport processes, with the latter being the most important reason (Mauder

et al., 2020). The energy balance closure (EBC) can be estimated as the fraction of turbulent heat fluxes to the available energy:

$$EBC = \frac{LE + SH}{R_n - G} \tag{2.12}$$

EBC can be visualized by plotting the turbulent heat fluxes against the available energy and fitting a regression curve. The slope of the linear regression model provides a value for energy closure, but the value depends on the type of regression model used. Orthogonal distance regression (ODR) is used in this study, since it accounts for errors in both axes, although an orthogonal least squares regression (OLS) is often used as well. Furthermore, the EBC can be formulated using the imbalance (imb) term, which contains all neglected effects and uncertainties, e.g. advection terms, thermal processes, vertical divergence of fluxes and uncertainties in experimental display (Mauder et al., 2020):

$$R_n - (SH + LE + G) = imb \tag{2.13}$$

Snow cover and its interannual variability strongly impacts energy exchange and land-atmosphere interactions in the Arctic, but the exact effects are unknown (Stiegler et al., 2016). Snow has a high albedo; it effectively reflects the downwelling shortwave radiation, which leads to smaller surface energy balance components (Stiegler et al., 2016). Further, snow has high emissivity and low thermal conductivity, making it an efficient thermal insulator (Lackner et al., 2022). Moreover, as the snow melts, soil water content increases, which affects future turbulent heat fluxes. Stiegler et al. (2016) found that in an Arctic heath ecosystem, abundant snow accumulation during winter caused larger latent and ground heat fluxes during summer due to increased soil water content. To analyze the energy budget on the snow surface, measurements of thermal conductivity and temperature of snow close to the surface are needed (Lackner et al., 2022).

3. Methods

In this chapter, the study site characteristics and the measurement system are introduced. Furthermore, the chapter contains all necessary information about the methods used in data processing

3.1 Site characteristics

The eddy-covariance tower is located in Kilpisjärvi in a valley between fells Saana and Korkea-Jehkats in a relatively topographically homogeneous area (20.79747°E, 69.0628°N), see Figure 3.1. Kilpisjärvi is a subarctic tundra site where evergreen shrubs are expanding. Species composition is dominated by an evergreen subshrub *Empetrum nigrum* and a deciduous shrub *Betula nana*. From the perspective of the EC-tower, the tallest shrubs lie in northwest. Some mosses and junipers are present in the footprint area as well. The soil consists of moraine and extends approximately one meter deep. Permafrost is present in the bedrock. Snow was occasionally present after the end of September, but a permanent snowpack formed as late as mid-November. According to the Finnish Meteorological Insitute, thermal winter began on October 29th in Kilpisjärvi in 2024 (Finnish Meteorological Institute, n.d.). Henceforth, the period covering August-October is defined as autumn and the period covering November-January is defined as winter.

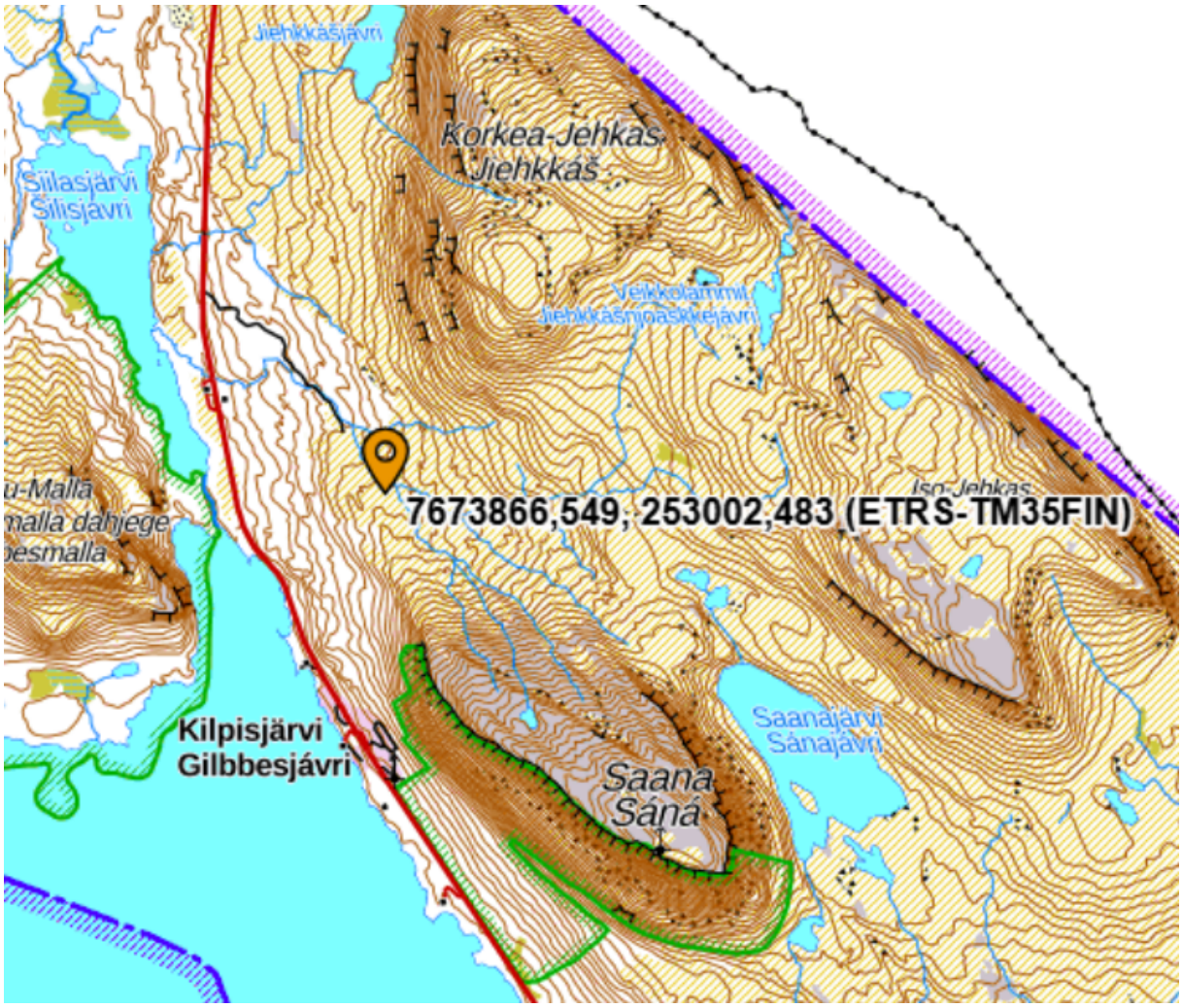

Figure 3.1: Map showing the location of the eddy covariance tower with an orange tap. Picture is obtained from map services of National Land Survey of Finland (National Land Survey of Finland, n.d.).

Figure 3.2 shows that most of the time the wind blew from southeast, from the direction of Saana, although some contribution comes from west-northwest as well. In theory, at nighttime the wind should blow downhill from slopes, whereas in daytime, the situation should be reversed. However, the day- and nighttime wind roses are very similar, possibly implying katabatic flows, which have strong wind shear near the surface, shallow maximum wind speed and large temperature gradients. The constant flux layer is suppressed in case of katabatic flows, making EC-derived turbulent heat fluxes unrepresentative of surface characteristics (Lord-May & Radić, 2024).

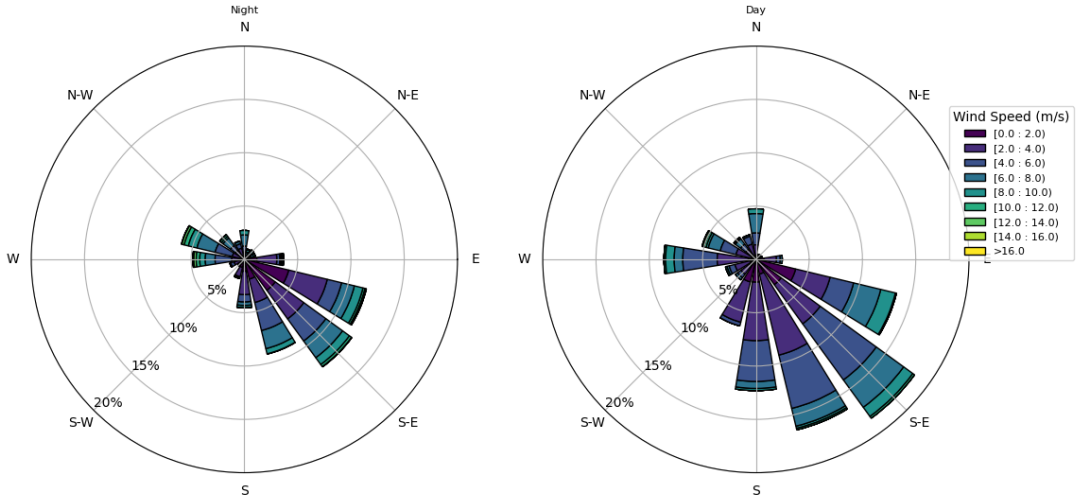

Figure 3.2: Wind roses for day- and nighttime compiled of 30 min data from the whole measurement period. Legend shows the wind speed.

3.1.1 Equipment setup

The eddy covariance tower is equipped with an enclosed infrared gas analyzer Li-Cor LI-7200RS and a 3D sonic anemometer Metek u-sonic-3 Scientific, which both have a sampling frequency of 10 Hz. The flow rate for Li-Cor is 10 LPM, sampling tube length is 0.80 m and the inner diameter of the sampling tube is 46 mm. The measurement height is 3.1 m, and the sensor separation between the gas analyzer inlet and the sonic probe is 3.5 cm. The inlet tube for Li-Cor is heated, whereas the anemometer is not.

Meteorological sensors are measuring air temperature and relative humidity at two heights (1.1 m and 3.1 m), PAR, incoming and outcoming short- and longwave radiation, air pressure, soil temperature at 4 depths (5, 10, 15 and 30 cm), soil moisture at 3 depths (5, 15 and 30 cm) and soil heat flux. The soil heat flux sensor is at 7.5 cm depth. The net radiometer sensors have been checked regularly in case of snow cover to obtain reliable radiation measurements.

3.1.2 Eddy covariance footprint

The footprint climatology was estimated using a two-dimensional model presented by Kljun et al. (2015). The model uses measurement height, roughness height (0.03 m), mean wind speed, wind direction, boundary layer height (800 m), Obukohv length, friction velocity and standard deviation of horizontal wind (v) as input parameters.

Boundary layer height was assumed constant throughout the period, since its variability does not significanlty alter the surface layer conditions above such short vegetation. The tower is only 3.1 meters tall, making its footprint quite small as well. Nearly all data comes from 25 meters radius, indicating that the surrounding fells are far enough to not cause significantly distorted flow patterns at the study site. Overall, the shape of the footprint looks very similar to that of the wind roses; a large fraction of data originates from the southwest.

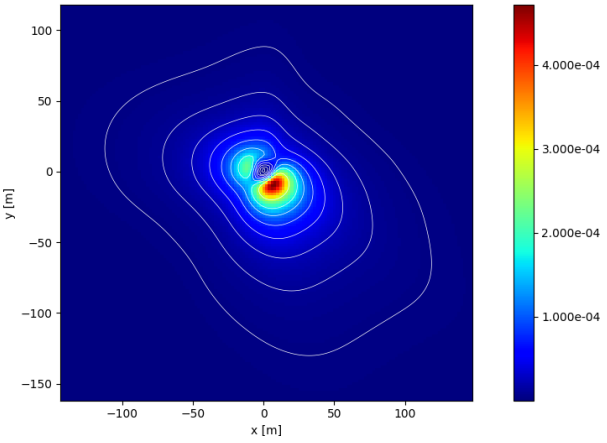

Figure 3.3: Footprint climatology of the eddy covariance tower adapted from Natali et al. (2019). The colors indicate how strongly each square meter of surface contributes to the measured flux – red having the most influence and blue having the least. Contour lines represent percentages of source areas ranging from 10%–80%.

3.2 Data processing

3.2.1 Preprocessing of eddy-covariance data

The data was preprocessed using EddyUH software developed at the University of Helsinki by Peltola and Mammarella (2015). The coordinate rotation was done using the double rotation method presented in Aubinet et al. (2012). Detrending was done using block averaging and the maximum number of spikes allowed was 18. Crosswind correction was applied to sonic temperature. The mean lag time for CO_2 was 1 second and 0.30 seconds for water vapor and temperature. Time lag was corrected with the maximum cross-covariance method. Time lag optimizer was calculated only for August–September data due to stronger signal, as were transfer functions. Flux quality criteria for CO_2 and H_2O were defined according to (Mauder et al., 2013) so that

Flag 0 (high-quality): FST $<$ 0.3 and 1 $<$ kurtosis $<$ 8 and -2 $<$ skewness $<$ 2

Flag 1 (moderate quality): FST $<$ 1 and 1 $<$ kurtosis $<$ 8 and -2 $<$ skewness $<$ 2

Flag 2 (low-quality): Everything else,

where FST stands for flux stationarity. Only CO_2 fluxes flagged with 0 or 1 were used in further analysis, although the use of FST criteria causes several sub-zero data points to vanish. For water vapor, data was not filtered according to flags.

3.2.2 Data postprocessing

The night flux error discussed in section 2.2 causes an overestimation of carbon sequestration since it mostly affects nighttime measurements (Aubinet et al., 2012). The significance of the error depends on meteorological conditions, topography, land cover heterogeneity and soil and plant biology (Aubinet et al., 2012). It is generally corrected by finding a friction velocity threshold under which the CO_2 flux begins to decrease. In this study, friction velocity values under 0.2 $\mathrm{m\,s^{-1}}$ were filtered out. Although there are no clear patterns on months October-January, the filtering was applied to all months to ensure coherent data management. The figure showing monthly nighttime CO_2 flux with respect to friction velocity is presented in Appendix A.1

The storage fluxes for SH, LE and CO_2 were calculated as

$$J_{SH} = c_p * (\overline{\rho_{d_1}} * \frac{\Delta T_1}{\Delta t} * \Delta z_1 + \overline{\rho_{d_2}} * \frac{\Delta T_2}{\Delta t} * \Delta z_2) \tag{3.1}$$

$$J_{LE} = L_v * (\overline{\rho_{d_1}} * \frac{\Delta q_1}{\Delta t} * \Delta z_1 + \overline{\rho_{d_2}} * \frac{\Delta q_2}{\Delta t} * \Delta z_2) \tag{3.2}$$

$$J_{CO_2} = \frac{\overline{\rho_{d_2}}}{M_d} * \frac{\Delta c}{\Delta t} * z_2 \tag{3.3}$$

where c_p is the heat capacity of air in constant pressure, ρ_d is the dry air density, ΔT is air temperature gradient, Δt is the time interval (1800 seconds), Δz is the difference between measurement heights, L_v is the latent heat of water vaporization, Δq is the specific humidity gradient and M_d is the molar mass of dry air (28.964 g/mol). The lower indices correspond to measurement heights 1 (1.1 m) and 2 (3.1 m). Specific humidity was calculated using average air pressure, temperature and relative humidity. Temperature and relative humidity were measured at two heights, while there was only one measurement height of CO_2 mixing ratio available. Biomass and soil storage terms were neglected in this study.

The storage fluxes have very small values, as is expected due to short vegetation and measurement height. The values range from [-0.41 – 0.22] $\mu\mathrm{mol\,m^{-2}s^{-1}}$ for CO_2, [-4.26 – 4.70] $\mathrm{W\,m^{-2}}$ for SH and [-4.49 – 4.79] $\mathrm{W\,m^{-2}}$ for LE. Storage fluxes for SH and LE were similar throughout the months, while the storage flux of CO_2 had more fluctuations in the first two months of the measurement period, when photosynthesis was still active. The effect of snowpack on storage fluxes was ignored due to negligible impact. The storage fluxes were added to the original data, and all fluxes presented here contain the storage correction.

Flux partitioning was done by fitting an exponential regression curve to nighttime CO_2 flux vs. soil temperature (at 5 cm) plot for the whole measurement period where only positive values of CO_2 flux were approved. The figure is presented in Appendix A.2. The obtained regression parameters were used to quantify ER and GPP during

daytime. GPP was forced to be negative, since some positive values occured. The mean difference between modelled and measured NEE was 1.35 μmol m^{-2}s^{-1}, which means that respiration is overestimated. The maximum difference was 22.17 μmol m^{-2}s^{-1}, which is caused by a small number of outliers and does not introduce systematic bias

3.2.3 Gapfilling

Soil temperature was gapfilled by linear interpolation since the fluctuations were rather small and the gaps were short. Air temperature was gapfilled by comparing it with data from the Finnish Meteorological Institution (FMI, (Finnish Meteorological Institute, n.d.)) collected a few kilometers from the EC tower, applying an OLS fit and normalizing the FMI data with the acquired slope. The missing values were then obtained from the normalized FMI data. PAR was gapfilled by linear interpolation in case of a short gap, and by using mean diurnal values of surrounding days, if the gap was several hours or days long. The mean diurnal -method yielded rather adequate results, but introduces uncertainty especially during long gaps, since there was no information of e.g. cloudiness available.

Turbulent heat and CO_2 fluxes contained gaps ranging from hours to days. While sensible and latent heat fluxes were not gapfilled, CO_2 flux was gapfilled using a random forest machine learning technique. The model was first trained with non-gapfilled values of PAR, air temperature at 3.1 m and soil temperature at 5 cm. 100 training trees were used and the random state was arbitrarily chosen to be 42. Gapfilled PAR, air temperature and soil temperature were used in making the final predictions. Overall 4328 values were predicted. The original dataframe contained 8060 rows, so CO_2 flux data had a large number of gaps, with some exceeding a week. Furthermore, the relationships between fluxes and environmental variables were examined by calculating the Pearson correlation coefficent and with visual inspection.

4. Results

This chapter first briefly evaluates the performance of random forest. Next, the evolution of meteorological variables and CO_2 flux is presented, and dependence between them is introduced. Subsequently, flux partitioning results are discussed and lastly, the radiation conditions and energy balance are investigated.

4.1 Random forest performance evaluation

By visual inspection, random forest seems to perform quite well in gapfilling the CO_2 flux (see Fig. 4.1); it follows the original flux pattern and diurnal cycle is visible. The model performance was evaluated by splitting the dataset into an "unseen" test set before training the model, which contained 20% of the original flux data. The comparison between original and predicted flux values are shown in Figure 4.2. The R^2 value and root mean squared error were 0.77 and 0.75 μmol $m^{-2}s^{-1}$, respectively, suggesting that the model was able to gapfill the flux sufficiently accurately.

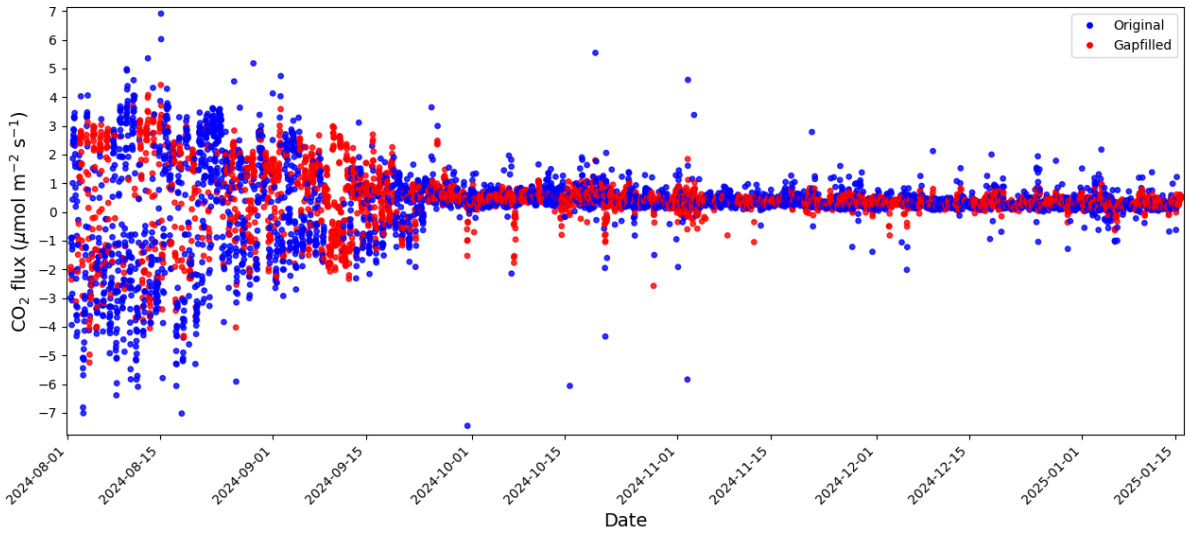

Figure 4.1: The original half-hourly CO_2 flux in blue and the predicted flux in red.

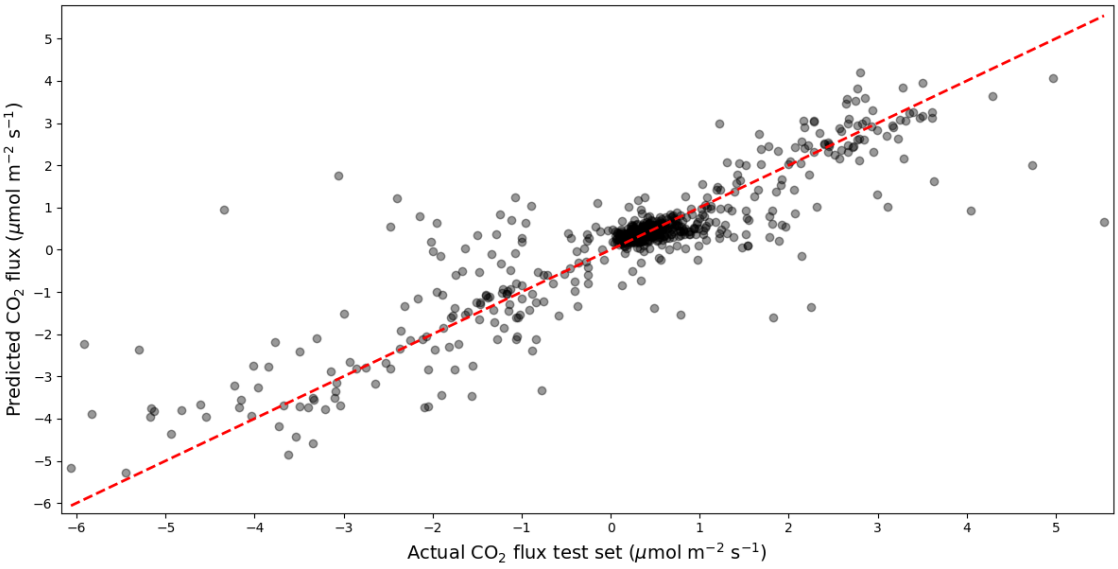

Figure 4.2: Comparison between the original CO_2 flux and the modelled flux between the test set. 1:1 line shown in red.

4.2 Temporal evolution of climate variables

Figure 4.3 shows the evolution of soil and air temperature, snow depth and PAR during the measurement period. During autumn, air temperature fluctuated between -9°C and 22°C. Soil temperature follows its diurnal pattern with a small lag, and fluctuates between 0°C and 17°C. Halfway through September air temperature reaches its first zero values, and drops permanently to sub-zero ranges at the end of September, when the first snowfall occurs. Concurrently, soil temperature fluctuations are significantly reduced. Soil temperature stays positive but very close to zero until the end of November, when it turns negative – although still being very close to zero. Deeper soil layers had colder temperatures until the middle of September, until the strafication changed; during winter the warmest temperatures were detected in the deepest layers (not shown). Air temperature ranged from -23°C to 10°C and soil temperature ranged from -1°C to 0°C during winter. A permanent snowpack begins to form halfway through November, which is exceptionally late for the location. Snow melting occurs occasionally, but the snowpack reaches a height of one meter during January.

PAR begins to decrease rather linearly from the beginning of August. PAR has a distinct diurnal cycle, but the maximum values vary between days due to differences in cloudiness. The maximum value of PAR during the whole measurement period, approximately 1250 μmol m^{-2}s^{-1}, was reached during August. From the middle of November to the end of the measurement period PAR is approximately zero.

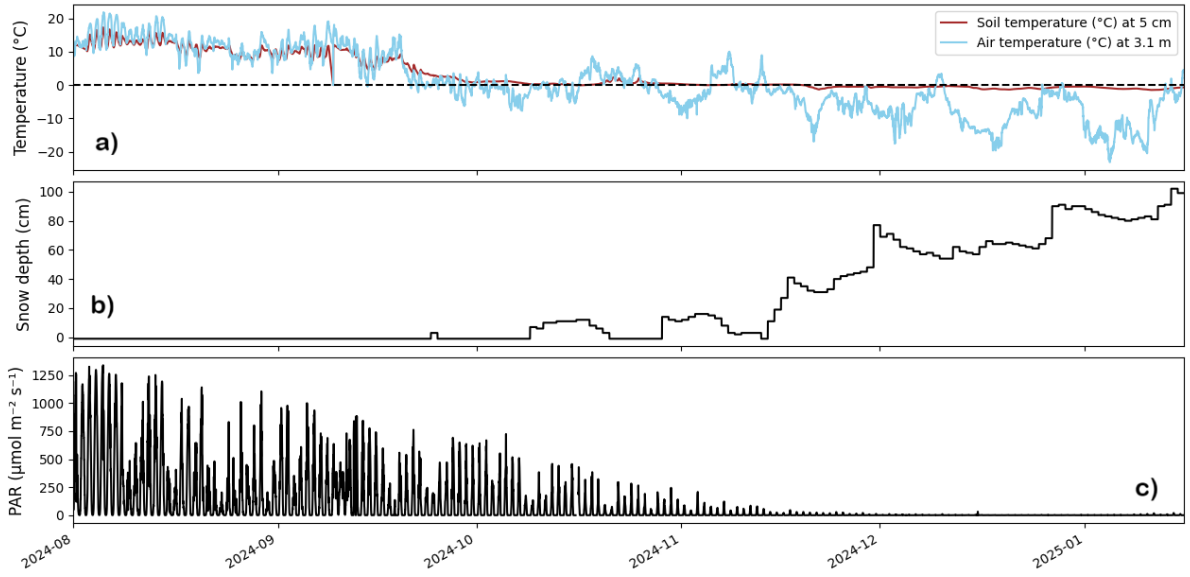

Figure 4.3: Time series of a) air and soil temperature, b) snow depth and c) PAR during the measurement period.

4.3 Diurnal variation of CO_2 flux, air temperature and photosynthetically active radiation

Figure 4.4 shows the monthly diurnal cycle of CO_2 flux with ± 1 standard deviation and Figure 4.5 presents the diurnal cycles of PAR and air temperature on each month. CO_2 flux has a distinct diurnal pattern in August and September: negative values appear during 06–18 in and the maximum negative value (-2.60 μmol m^{-2}s^{-1} in August and -1.07 μmol m^{-2}s^{-1} in September) is reached at 11 AM when PAR peaks. The standard deviation of the flux shows largest values during the day perhaps due to the sensitivity of photosynthesis to PAR; the amount of assimilated carbon varies between days due to differences in cloudiness. From October to January, the diurnal cycle of CO_2 flux disappears and the mean values are extremely small, but positive throughout the day (from 0.06 μmol m^{-2}s^{-1} to 0.842 μmol m^{-2}s^{-1}). The mean flux turns out to be positive throughout the winter. Temperature is generally highest during the evening in winter, but the changes in mean value are very small.

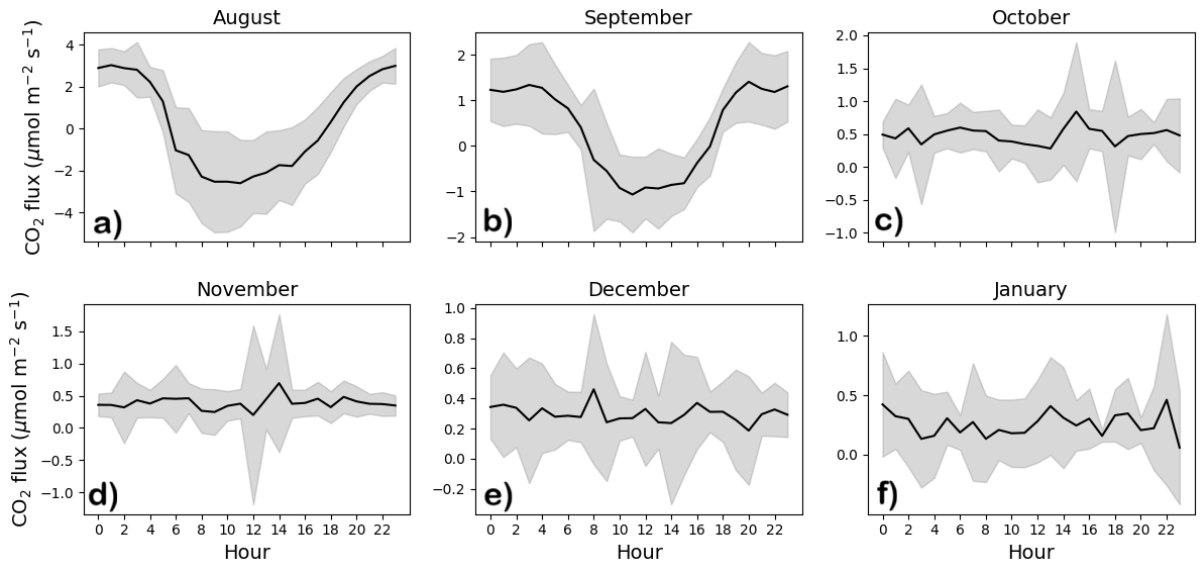

Figure 4.4: Average diurnal CO_2flux for each month. Shaded areas represent the ±1 standard deviation from the mean.

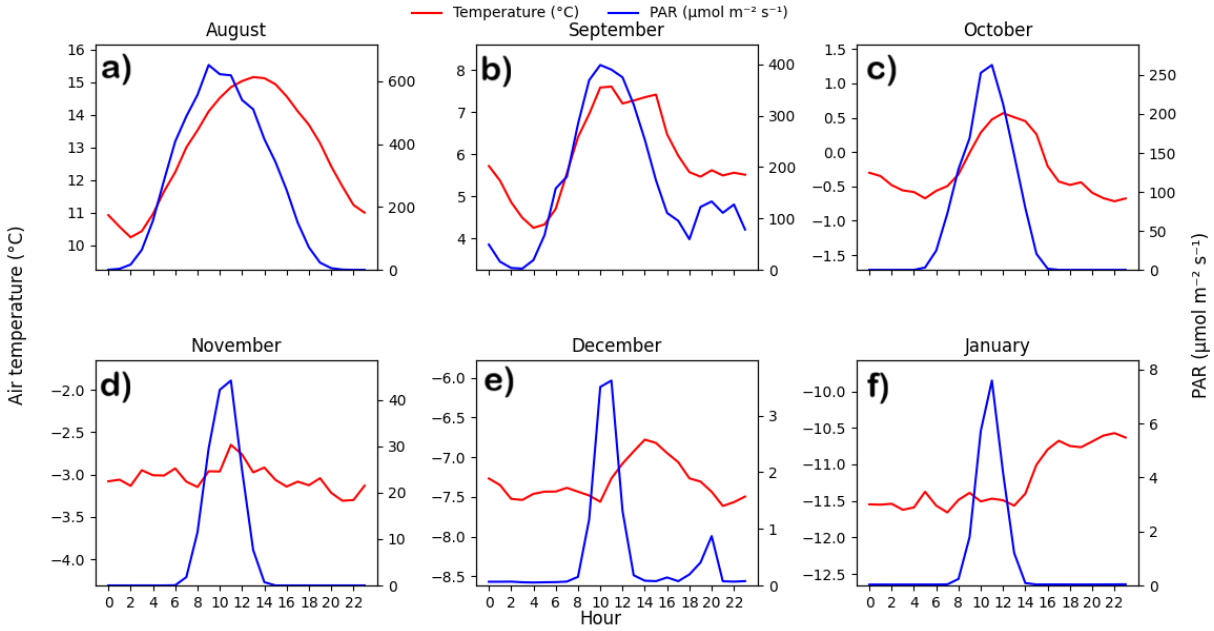

Figure 4.5: Average diurnal PAR (blue) and air temperature (red) for each month.

4.4 Factors controlling CO_2 flux

Comparisons of soil and air temperature, RH and PAR to CO_2 flux were done separately for autumn and winter months to observe possible differences in seasonal relationships. The results with Spearman correlation coefficents and p-values are shown in Figure 4.6. If the p-value is smaller than 0.05, the result is seen as statistically significant.

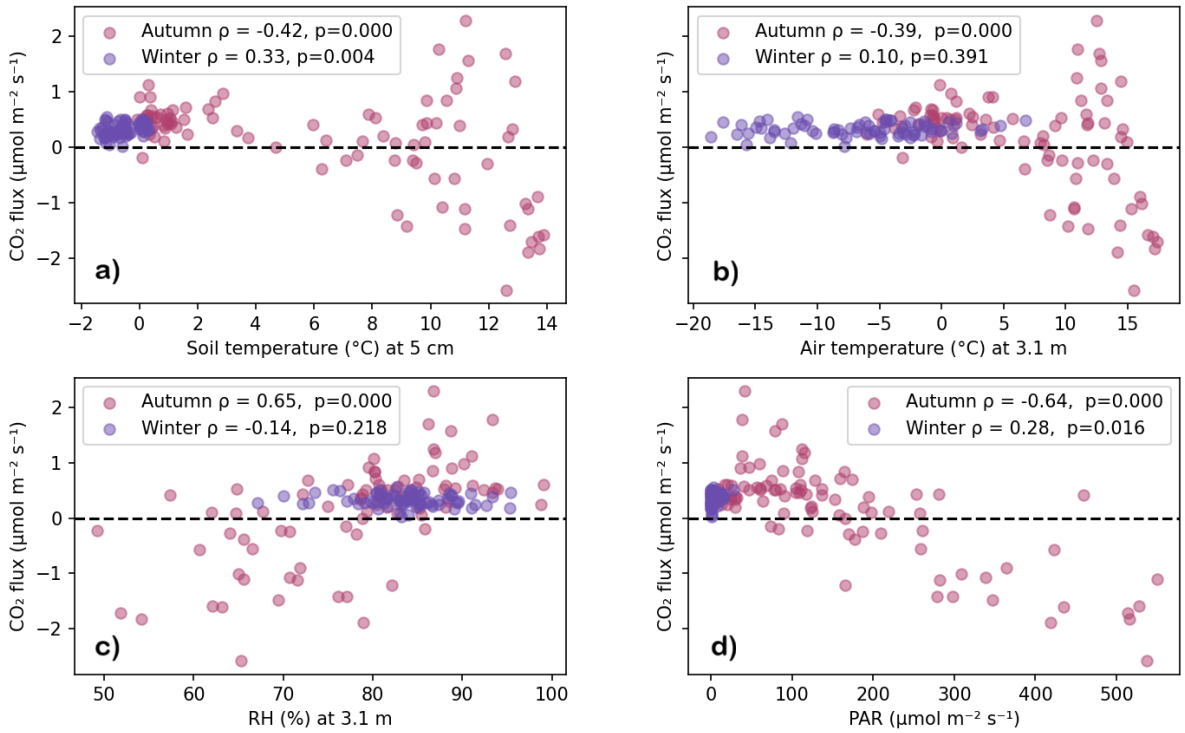

Figure 4.6: CO_2 flux with respect to a) soil temperature, b) air temperature, c) RH and d) PAR with Spearman correlation coefficents and p-values during autumn and winter. Values are daily averages.

There is no significant correlation between the variables and the flux during winter, apart from soil temperature. The Spearman correlation coefficent for soil temperature and CO_2 flux is 0.33 in winter, with a p-value of 0.004. On the contrary, during autumn all the presented variables significantly correlate with the flux, with PAR having the strongest negative correlation (ρ = -0.64) and RH having the strongest positive correlation (ρ = 0.65). Soil and air temperature have a negative correlation with CO_2 flux with correlation coefficents of ρ = -0.42 and ρ = -0.39, respectively. As the temperature increases, CO_2 flux disperses as both photosynthesis and respiration rates increase. Negative correlation indicates that photosynthesis increases more with temperature than respiration, leading to overall more uptake of CO_2 than release. Only negative flux values are present after soil temperature rises to 13°C and air temperature to 15°C. These values are reached during the day when photosynthesis takes place.

While there is no wintertime correlation between CO_2 flux and RH, they correlate positively in autumn with a correlation coefficent of ρ = 0.65. As RH reaches 90%, only positive flux values are present, whereas negative flux values appear with lower RH. Lowest RH values in autumn are observed during the day. The correlation of CO_2 flux and PAR behaves similarly: negative correlation during autumn is caused by increased photosynthesis during the day, whereas wintertime correlation is insignificant since PAR is limited.

4.5 Net ecosystem exchange and cumulative CO_2 flux

Flux partitioning was done to see the relative contribution of photosynthesis and respiration. Figure 4.7 shows the time series of GPP and ER during the measurement period. Both have a distinct diurnal cycle during the first two months which dampens in the winter. The greatest GPP in autumn is -11.1 μmol m^{-2}s^{-1} and the maximum ER is 7.4 μmol m^{-2}s^{-1}. GPP declines quite linearly from August to the end of September, whereas ER exhibits more fluctuations. At the end of September, GPP is already very close to zero. It shows some anomalously large peaks in October and November which are likely produced by errors in preprocessing. The November peak is notably abnormal, given that temperature is low and snowpack has formed; carbon assimilation should not be that substantial. Altogether, GPP remains very low or zero during winter, and ER is the dominating component (maximum 4.6 μmol m^{-2}s^{-1}), which causes an overall positive NEE during the six month period.

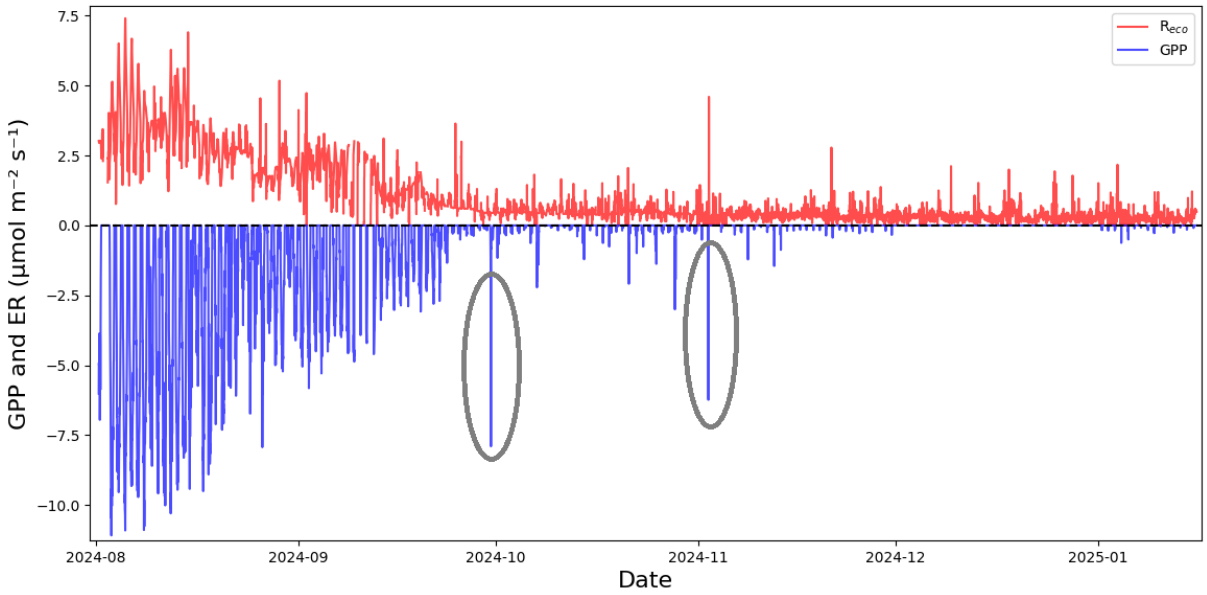

Figure 4.7: Time series of GPP and ER partitioned using the nighttime approach with gray circles emphasizing the questionable values.

The cumulative CO_2 flux reveals the amount of carbon gained or released during the measurement period. Figure 4.8 presents the time series of the cumulative flux and monthly ranges of NEE. The cumulative flux decreases until the end of August, when it begins to increase and becomes positive. Despite the large GPP in August, the median NEE is slightly positive. The flux displays minor fluctuations until the end of September due to diurnal variation. The diurnal variations are not visible anymore after October, as was shown in figure 4.4. The cumulative flux increases virtually linearly throughout

winter, reaching its maximum value of 55.4 $\mathrm{gC\,m^{-2}}$ at the end of the measurement period. While staying very close to zero, the median NEE remains positive throughout the measurement period.

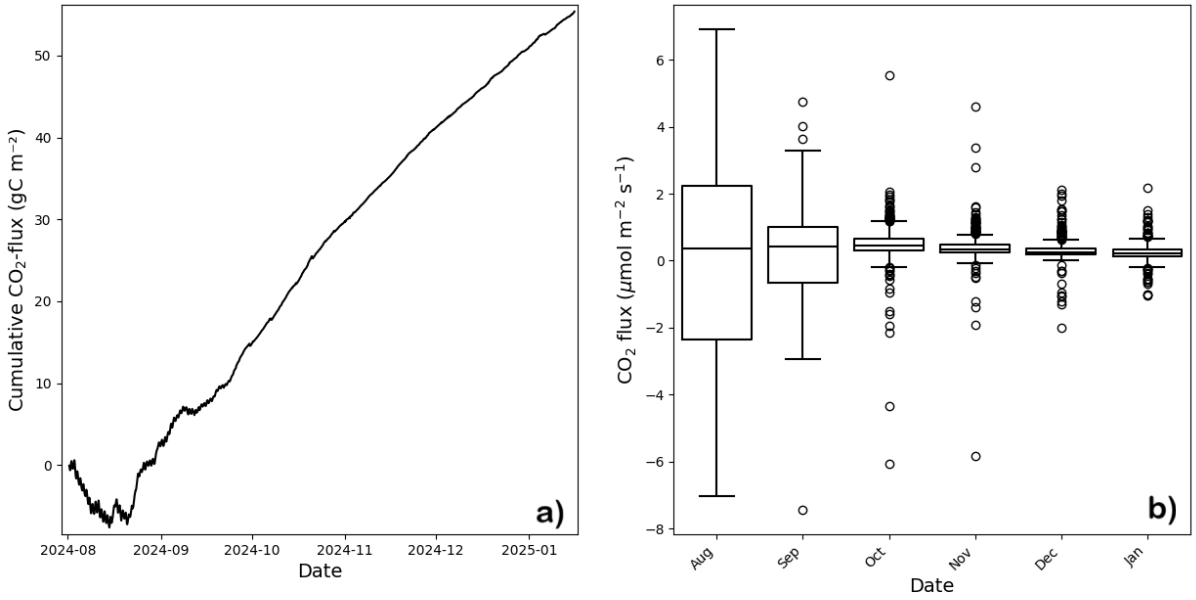

Figure 4.8: a) All time cumulative CO_2 flux and b) monthly ranges of CO_2 flux (non-gapfilled data).

4.6 Radiation conditions and energy balance

The polar night lasted in Kilpisjärvi from 25.11. to 15.1. in 2024-2025 study period. During this period, net longwave radiation exceeds the net shortwave radiation due to absence of sunlight and high albedo and emissivity of the snow cover. Thus, the net radiation remains negative throughout the polar night. Figure 4.9 shows the mean diurnal energy components for each month.

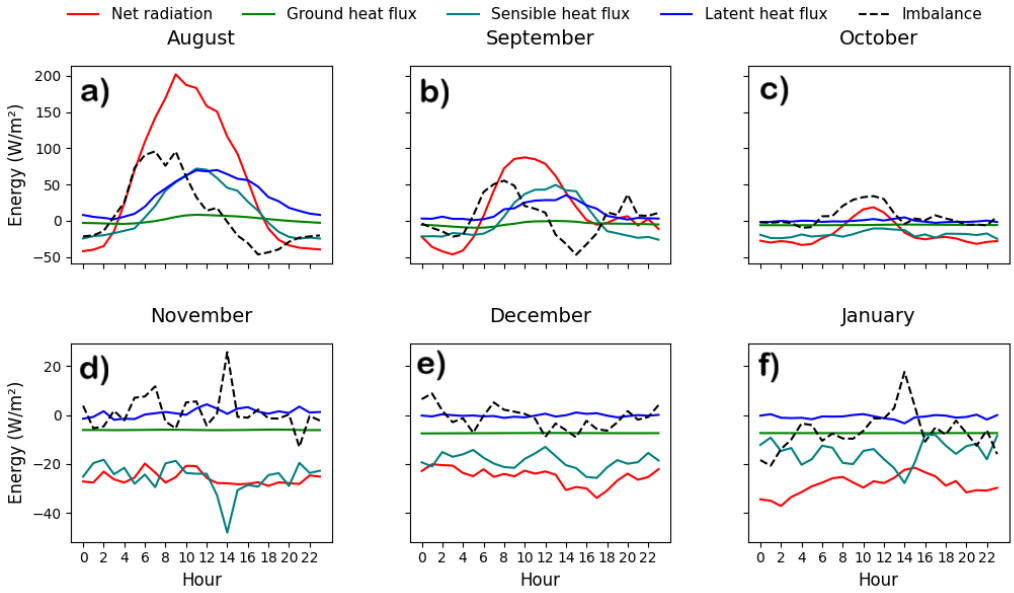

Figure 4.9: Average diurnal energy components for each month. Note the y-axis scale is much smaller in figures d), e) and f).

The general diurnal cycle of energy components is visible in August and September: net radiation reaches its peak around midday and turns negative during the night. The turbulent heat fluxes are approximately the same order of magnitude with each other during the day, and both peak soon after net radiation. Mean diurnal LE stays positive throughout the day, while SH becomes negative during the night as the ground cools after sunset. Positive LE implies evaporation is taking place and cooling the surface. In October, LE and SH are both negative but very close to zero. During the whole autumn period, mean LE and SH are 17.0 $\mathrm{W\,m^{-2}}$ and 0.4 $\mathrm{W\,m^{-2}}$, respectively, and the mean net radiation is 18.1 $\mathrm{W\,m^{-2}}$. The ground heat flux is very small, but shows a minor peak during the afternoon as well during August and September; the maximum value is lagging approximately two hours from the net radiation maximum.

The diurnal heat fluxes grow more negative as the months progress, until November. The diurnal mean of net radiation is -26 $\mathrm{W\,m^{-2}}$ in the winter. Mean diurnal SH turns out to be negative as well throughout October-January, and has largest negative values in November afternoon. The lack of sunlight causes the ground to cool due to longwave emissions, making the air directly above the surface warmer. SH is thus directed from the air into the surface. Positive values of SH occur occasionally during the polar night. LE is negligibly small during the winter, and fluctuates at subzero ranges. During winter months, the mean LE is 0.1 $\mathrm{W\,m^{-2}}$ and the mean SH is -20.8 $\mathrm{W\,m^{-2}}$. The mean ground heat flux is negative throughout the six month period, ranging from - 2.9 $\mathrm{W\,m^{-2}}$ in autumn to -6.9 $\mathrm{W\,m^{-2}}$ in winter.

The EBC composed of daily average energy components is presented in Figure 4.10.

Daily means are used since according to Foken and Nappo (2008), longer averaging times often yield higher closure. The best closures were achieved in August (91%), November (90%) and September (86%), whereas other months exhibited much lower closure. The lowest value was in January (13%).

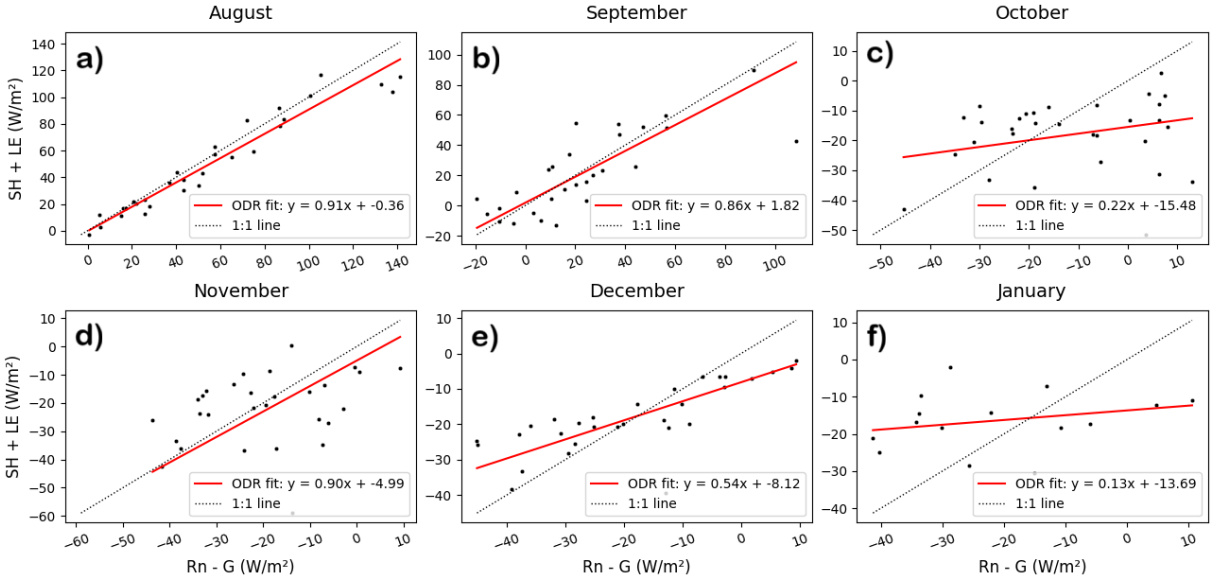

Figure 4.10: Energy balance closure for each month derived from daily averages. Note the different y-axis scale between upper and lower subplots.

5. Discussion

During August and September the available PAR and sufficient air temperature allow photosynthesis during daytime. This induces a distinct diurnal cycle of CO_2 flux, which was significantly reduced in October and disappeared completely during the following months. In October, respiration begins to dominate photosynthesis even though PAR is still around 300 μmol m^{-2}s^{-1} during the day. In contrast, air temperature is mainly negative (average temperature is -0.2°C) and snow cover is present part of the month. Thus, photosynthesis may be limited by temperature and snow, which covers part of the vegetation. During autumn the mean air temperature is 6.2°C. Despite the very small values during November-January, the mean CO_2 flux remains positive (0.38 μmol m^{-2}s^{-1}); respiration in the soil takes place throughout the winter. The snowpack allows the soil to maintain a relatively warm and steady temperature, enabling microbial decomposition to continue; the average soil temperature at 5 cm depth during winter is -0.6 °C, while the average air temperature is -6.4°C. The maximum difference between soil and air temperature is nearly 20°C. Since snow depth directly affects soil temperature and defines the length of winter, the regional patterns of total wintertime respiration could potentially be estimated with maximum snow depth, as was suggested by Grogan and Jonasson (2006).

The relationship between PAR, RH and air and soil temperature to CO_2 flux were investigated separately for autumn and winter periods. During autumn, all variables are statistically significant drivers of CO_2 flux. PAR has the largest negative correlation coefficent (ρ = -0.64) followed by soil temperature (ρ = -0.42) and air temperature (ρ = -0.39), while RH has the largest positive correlation coefficent (ρ = 0.65). During winter soil temperature is the only statistically significant driver (p = 0.004) with a correlation coefficent of ρ = 0.33. It is noteworthy that the correlation is positive despite being negative in autumn – increase of soil temperature during winter only increases respiration, since photosynthesis is limited by other factors. While Oechel et al. (2014) reported soil temperature to be an important driver during autumn, they found no significant relationship between wintertime fluxes and temperature in Alaska's North Slope tussock-tundra. Nonetheless, Mavrovic et al. (2023) identified soil temperature as the most significant controller of winter CO_2 fluxes while the soil was fully frozen across measurement sites

in Northern Canada. Similarly Webb et al. (2016) reported soil temperature to be the key driver of winter CO_2 emissions in an Alaskan tundra site. In Kilpisjärvi the soil temperature remains relatively constant throughout the winter, which presents difficulties in observing correlations.

Respiratory losses in August are sufficiently low to allow the cumulative CO_2 flux to decrease. GPP has its maximum value in August (11.1 μmol m^{-2}s^{-1}) after which it declines rapidly and reaches first near-zero values at the end of September. While GPP is virtually nonexistent during the winter (cumulative sum 0.7 gC m^{-2}), it still shows some negative peaks at relatively small PAR values, which are likely produced by errors in data processing. ER maximum is similarly achieved in August (7.4 μmol m^{-2}s^{-1}). The cumulative flux during winter is 25.6 gC m^{-2} in Kilpisjärvi – higher than what was observed by Oechel et al. (2014) in an Alaskan moist acidic tussock tundra ecosystem, where the wintertime carbon exchange was 13 $\pm$ 0.7 gC m^{-2}. Similarly the autumn fluxes are higher at Kilpisjärvi (29.8 gC m^{-2}) than in Alaska (16$\pm$0.7 gC m^{-2}). However, soil and air temperature are lower in Alaska in both seasons, and the vegetation composition is different. Overall, the cumulative NEE during the whole measurement period is 55.4 gC m^{-2}. The results are smaller than what Euskirchen et al. (2012) observed at a Northern Alaska heath tundra site: GPP ranged from -3 to- 7 gC m^{-2} and ER ranged from 67 to 118 gC m^{-2} during 4 consecutive winters, while the wintertime cumulative flux ranged from 105-119 gC m^{-2} during two years. However, their winter lasted from September to May. It is probable that the cumulative flux in Kilpisjärvi would be of the same order of magnitude were all the winter months included, given that winter typically continues until April-May.

Comparable cumulative CO_2 flux has been predicted before by Watts et al. (2019). They produced a gridded dataset containing non-growing season (September–April) soil CO_2 flux from 2003 to 2018 across Arctic and boreal regions. Moreover, they calculated predictions for years 2017-2100. The dataset was produced by applying a Boosted Regression Tree machine learning algorithm to in situ observations of CO_2 fluxes. These predictions were made under Representative concentration pathways (RCP) 4.5 scenario, which assumes a radiative forcing of 4.5 W m^{-2} by the year 2100. The closest coordinates to Kilpisjärvi measurement station were (69.08931°, 20.67620°). For the given area, they predicted a total winter CO_2 flux for 2024-2025 to be 93.37 gC m^{-2}. The lowest value was obtained in February and the highest in March. Including only the time period from September to January, the cumulative flux was 52.4 gC/m^2, which is very similar to the results obtained in this study. The similarity suggests that the model was able to accurately predict the evolution of warming and its effects on Kilpisjärvi area leastwise in near-future.

The evolution of energy components in Kilpisjärvi during winter are partially similar

to what has been observed in other Arctic ecosystems. The largest difference is in ground heat flux. While G is very small in Kilpisjärvi throughout the measurement period, Langer et al. (2011) measured a significant ground heat flux during the winter in a northern Siberian polygonal tundra site. They showed that G balanced approximately 60% of radiative losses during early- and mid-winter. The dissimilar result is likely explained by the site characteristics: the maximum snow depth was close to 20 cm, vegetation composition is different, and the site experiences much colder winters than Kilpisjärvi. However, in late winter they observed SH to balance most of the radiative losses, while G decreased. The late winter conditions in the Siberian site seem to be similar to the whole wintertime in Kilpisjärvi, where SH counterbalances most of the negative net radiation (wintertime mean is -21 $\mathrm{W\,m^{-2}}$). Alternatively, Lackner et al. (2022) observed a significant negative SH throughout the winter in a shrub-tundra site in eastern Canada where the environment is comparable to Kilpisjärvi site. Both studies confirm a negligible LE during winter, in line with the observations done in Kilpisjärvi, where the mean LE in winter is 0.1 $\mathrm{W\,m^{-2}}$.

The energy balance closure problem governs all EC-sites and is yet to be resolved; across CO_2 flux networks, an EBC of approximately 80% prevails (Aubinet et al., 2012). Currently there exists only few studies of the EBC in Arctic areas during non-growing season. In an Alaskan heat tundra, a closure of 90% was found during a period without snow cover, and 79% when snow was present (Euskirchen et al., 2012). The median EBC at FLUXNET polar sites has been 70%, the lowest of all represented ecosystem types (Cui & Chui, 2019). The estimation is based on daily data retrieved from FLUXNET15 database (see Pastorello et al. (2021)). There are only 16 sites available, most of which are wetlands. The low EBC was explained by instrument accuracy during cold temperatures and snowy conditions. In Kilpisjärvi the closure is best in August (91%), November (90%) and September (86%). While it is expected that the EBC is lower during winter, when snow is present and turbulent mixing may be weak, the low value observed in October (22%) is unexpected. Even though filtering of $u_* < 0.2\ \mathrm{m\,s^{-1}}$ was applied, incomplete turbulence conditions may have distorted the measurements to some degree. Sub-mesoscale transport is the main reason for EB non-closure (Mauder et al., 2020). Considering the Kilpisjärvi EC site is located between fjells, advection may have potentially affected the measurements, even though the footprint is rather small compared to the distance between fjells and the measurement system.

While Foken and Nappo (2008) emphasize the relatively high heat storage in the soil, it was assumed negligible in this study, which may have decreased the EBC. Measurements of thermal conductivity or snow temperature close to the surface were not available for the Kilpisjärvi site, so the lack of snow cover energy balance may result in offset of EBC as well. In contrast, the heat fluxes in snow are relatively small compared to the other

components of the EB, justifying the neglection (Weller & Holmgren, 1974). The high imbalance term seen in figure 4.9 likely stems from gaps in turbulent fluxes, and not filtering water vapor flux according to quality flags. Furthermore, Figure 3.2 revealed that a large fraction of the wind during day- and nighttime originates from southeast, where the fjell is located. This may be explained by katabatic flows. However, the data was not filtered according to the wind conditions, since it was not possible to explicitly investigate whether the flows are indeed katabatic.

Climate change in the Arctic will result in earlier springs and longer autumns. While GPP may increase due to earlier CO_2 uptake, warmer autumns are expected to increase ER, since plant dormancy is controlled by light, possibly offsetting the carbon gained during spring (Euskirchen et al., 2012). Even though photosynthesis is increasing with higher temperatures, expansion of the growing season and shrub enroachment, increasing respiration rates during winter and autumn may transform Arctic areas into annual carbon sources (Oechel et al., 2014). For example, Euskirchen et al. (2012) found that the wintertime CO_2 release exceeded the summertime uptake in a heath and a wet sedge tundra in Alaska. The results obtained here indicate that the Kilpisjärvi site is a carbon source during the non-growing season as well. Carbon losses in the Arctic during winter are thus likely to increase if global warming accelerates, although current obervations may not adequately reflect future environmental responses to warmer winter conditions (Natali et al., 2019). Year-round measurements are needed in high-latitude ecosystems to confirm the annual carbon balance. Estimating the amount of emissions that will be released into the atmosphere from the large soil carbon stocks and permafrost in the Arctic is critical considering the global carbon cycle. Since the carbon balance in the Arctic varies regionally, a more profound flux tower network is needed to get ecosystem-specific estimates of carbon exchange.

6. Conclusions

In this thesis the CO_2 exchange and energy balance of a subarctic ecosystem was studied using EC data collected during August–January in 2024–2025. Moreover, the effects of environmental variables to CO_2 fluxes was evaluated.

While the CO_2 flux in Kilpisjärvi showed a clear diurnal cycle in August and September, it grew close to zero as the months progressed. Respiration begins to dominate photosynthesis in October, and GPP is approximately zero during winter. Relatively warm soil temperatures allowed microbial respiration to take place throughout the winter, causing a positive CO_2 flux. The cumulative CO_2 flux for the whole measurement period was 55.4 $\mathrm{gC\,m^{-2}}$, which agreed relatively well with other studies made in the Arctic.

A permanent snowpack began forming in November. During the winter the lowest air temperatures were around -20°C. Furthermore, air temperature fluctuated a lot and was even occasionally positive during the polar night. In contrast, soil temperature was very stable during the winter, and remained close to zero due efficient insulation provided by the snow cover. The main drivers for CO_2 flux during autumn were PAR and RH, followed by soil and air temperature. During winter, soil temperature was recognized as the only statistically significant driver. The correlation was positive in winter and negative in autumn, indicating that warmer soil temperatures during winter solely increase respiration, whereas during autumn photosynthesis is increased as well.

The energy components exhibited a clear diurnal cycle on August and September: the turbulent heat fluxes peak soon after net radiation and the ground heat flux is very small. During winter, sensible heat flux balances the longwave radiation losses caused by negative net radiation, whereas latent and ground heat flux are negligible. Other studies confirm the impact of sensible heat flux in the Arctic during winter, as well as the negligible role of latent heat flux. The energy balance closure is approximately 90% in August and November, whereas other months showed lower closure.

Altogether, soil temperature drives the carbon emissions in winter, making the Kilpisjärvi site a carbon source due to warm soil allowing continuous respiration throughout the measurement period. Since the amount of growing season carbon uptake and the late-winter emissions are unknown, the annual carbon balance remains a question for future research.

Bibliography

Arndt, K., Hashemi, J., Natali, S., Schiferl, D., Luke, & Virkkala, A.-M. (2023). Recent advances and challenges in monitoring and modeling non-growing season carbon dioxide fluxes from the arctic boreal zone. *Curr Clim Change Rep*, *9*. https://doi.org/https://doi.org/10.1007/s40641-023-00190-4

Aubinet, M., Vesala, T., & Papale, D. (2012). *Eddy covariance a practical guide to measurement and data analysis*. Springer. https://doi.org/10.1007/978-94-007-2351-1

Cahoon, S. M. P., Sullivan, P. F., Shaver, G. R., Welker, J. M., & Post, E. (2012). Interactions among shrub cover and the soil microclimate may determine future arctic carbon budgets. *Ecology Letters*, *15*(12), 1415–1422. https://doi.org/https://doi.org/10.1111/j.1461-0248.2012.01865.x

Commane, R., Lindaas, J., Benmergui, J., Luus, K. A., Chang, R. Y.-W., Daube, B. C., Euskirchen, E. S., Henderson, J. M., Karion, A., Miller, J. B., Miller, S. M., Parazoo, N. C., Randerson, J. T., Sweeney, C., Tans, P., Thoning, K., Veraverbeke, S., Miller, C. E., & Wofsy, S. C. (2017). Carbon dioxide sources from alaska driven by increasing early winter respiration from arctic tundra. *Proceedings of the National Academy of Sciences*, *114*(21), 5361–5366. https://doi.org/10.1073/pnas.1618567114

Cui, W., & Chui, T. F. M. (2019). Temporal and spatial variations of energy balance closure across fluxnet research sites. *Agricultural and Forest Meteorology*, *271*, 12–21. https://doi.org/https://doi.org/10.1016/j.agrformet.2019.02.026

Elmendorf, S. C., Henry, G. H. R., Hollister, R. D., Björk, R. G., Bjorkman, A. D., Callaghan, T. V., Collier, L. S., Cooper, E. J., Cornelissen, J. H. C., Day, T. A., Fosaa, A. M., Gould, W. A., Grétarsdóttir, J., Harte, J., Hermanutz, L., Hik, D. S., Hofgaard, A., Jarrad, F., Jónsdóttir, I. S., ... Wookey, P. A. (2012). Global assessment of experimental climate warming on tundra vegetation: Heterogeneity over space and time. *Ecology Letters*, *15*(2), 164–175. https://doi.org/https://doi.org/10.1111/j.1461-0248.2011.01716.x

Eugster, W., Rouse, W. R., Pielke Sr, R. A., Mcfadden, J. P., Baldocchi, D. D., Kittel, T. G. F., Chapin III, F. S., Liston, G. E., Vidale, P. L., Vaganov, E., & Chambers, S. (2000). Land-atmosphere energy exchange in arctic tundra and boreal forest:

Available data and feedbacks to climate. *Global Change Biology*, *6*(S1), 84–115. https://doi.org/https://doi.org/10.1046/j.1365-2486.2000.06015.x

Euskirchen, E. S., Bret-Harte, M. S., Scott, G. J., Edgar, C., & Shaver, G. R. (2012). Seasonal patterns of carbon dioxide and water fluxes in three representative tundra ecosystems in northern alaska. *Ecosphere*, *3*. https://doi.org/http://dx.doi.org/10.1890/ES11-00202.1

Finnish Meteorological Institute. (n.d.). *Talvi 2024–2025 [winter 2024–2025]*. Retrieved October 6, 2025, from %7Bhttps://www.ilmatieteenlaitos.fi/talvi-2024-2025%7D

Foken, T., & Nappo, J. C. (2008). *Micrometeorology*. Springer.

Grogan, P., & Jonasson, S. (2006). Ecosystem co_2 production during winter in a swedish subarctic region: The relative importance of climate and vegetation type. *Global Change Biology*, *12*, 1479–1495. https://doi.org/doi:10.1111/j.1365-2486.2006.01184.x

Hobbie, S. E., Schimel, J. P., Trumbore, S. E., & Randerson, J. R. (2000). Controls over carbon storage and turnover in high-latitude soils. *Global Change Biology*, *6*(S1), 196–210. https://doi.org/https://doi.org/10.1046/j.1365-2486.2000.06021.x

Kaimal, J. C., & Finnigan, J. J. (1994). *Atmospheric boundary layer flows : Their structure and measurement*. Oxford University Press, Incorporated.

Kasurinen, V., Alfredsen, K., Kolari, P., Mammarella, I., Alekseychik, P., Rinne, J., Vesala, T., Bernier, P., Boike, J., Langer, M., Marchesini, L., Van Huissteden, K., Dolman, H., Sachs, T., Ohta, T., Varlagin, A., Rocha, A., Afrain, A., Oechel, W., . . . Berninger, F. (2014). Latent heat exchange in the boreal and arctic biomes. *Global Change Biology*, *20*, 3439–3456. https://doi.org/https://doi.org/10.1111/gcb.12640

Kljun, N., Calanca, P., Rotach, M., & Schmid, H. (2015). A simple two-dimensional parameterisation for flux footprint prediction (ffp). *Geoscientific Model Development*, *8*(11), 3695–3713. https://doi.org/10.5194/gmd-8-3695-2015

Lackner, G., Domine, F., Nadeau, F., Daniel, Parent, A.-C., Anctil, F., Lafaysse, M., & Dumont, M. (2022). On the energy budget of low-arctic snowpack. *The Cryosphere*, *16*, 127–142. https://doi.org/https://doi.org/10.5194/tc-16-127-2022

Langer, M., Westermann, S., Piel, K., & Boike, J. (2011). The surface energy balance of a polygonal tundra site in northern siberia – part 2: Winter. *The Cryosphere*, *5*, 509–524. https://doi.org/10.5194/tc-5-509-2011

Lasslop, G., Migliavacca, M., Bohrer, G., Reichstein, M., Bahn, M., Ibrom, A., Jacobs, C., Kolari, P., Papale, D., Vesala, T., Wohlfahrt, G., & Cescatti, A. (2012). On the choice of the driving temperature for eddy-covariance carbon dioxide flux partitioning. *Biogeosciences*, *9*, 5243–5259. https://doi.org/10.5194/bg-9-5243-2012

López-Blanco, E., Lund, M., Williams, M., Tamstorf, M. P., Westergaard-Nielsen, A., Exbrayat, J.-F., Hansen, B. U., & Christensen, T. R. (2017). Exchange of co in arctic tundra: Impacts of meteorological variations and biological disturbance. *Biogeosciences*, *14*(19), 4467–4483. https://doi.org/10.5194/bg-14-4467-2017

Lord-May, C., & Radić, V. (2024). Improved processing methods for eddy covariance measurements in calculating sensible heat fluxes at glacier surfaces. *Journal of Glaciology*, *70*, e84. https://doi.org/10.1017/jog.2024.39

Mauder, M., Cuntz, M., Drüe, C., Graf, A., Rebmann, C., Schmid, H. P., Schmidt, M., & Steinbrecher, R. (2013). A strategy for quality and uncertainty assessment of long-term eddy-covariance measurements. *Agricultural and Forest Meteorology*, *169*, 122–135. https://doi.org/https://doi.org/10.1016/j.agrformet.2012.09.006

Mauder, M., Foken, T., & Cuxart, J. (2020). Surface-energy-balance closure over land: A review. *Boundary-Layer Meteorology*, *177*, 395–426. https://doi.org/https://doi.org/10.1007/s10546-020-00529-6

Mavrovic, A., Sonnentag, O., Lemmetyinen, J., Voigt, C., Rutter, N., Mann, P., Sylvain, J.-D., & Roy, A. (2023). Environmental controls of winter soil carbon dioxide fluxes in boreal and tundra environments. *Biogeosciences*, *20*(24), 5087–5108. https://doi.org/10.5194/bg-20-5087-2023

McGuire, A., Anderson, L. G., Christensen, T. R., Dallimore, S., Guo, L., Hayes, D. J., Heimann, M., MacDonald, R. W., & Roulet, N. (2009). Sensitivity of the carbon cycle in the arctic to climate change. *Ecological Monographs*, *79*(4), 523–555. Retrieved July 30, 2025, from https://aquila.usm.edu/fac_pubs/1126

McLaren, R., Jennie, Buckeridge, M., Kate, van de Weg, J., Martine, Shaver, R., Gaius, Schimel, P., Joshua, & Gough, L. (2017). Shrub enroachment in artcic tundra: Betula nana effects on above- and belowground litter decomposition. *Ecology*, *98*, 1361–1376. http://www.jstor.org/stable/26165223

Mikan, J., Carl, Schimel, P., Joshua, & Doyle, P., Allen. (2002). Temperature controls of microbial respiration in arctic tundra soils above and below freezing. *Soil Biology and Biochemistry*, *34*(11), 1785–1795. https://doi.org/https://doi.org/10.1016/S0038-0717(02)00168-2

Montagnani, L., Gruenwald, T., Kowalski, T., Mammarella, I., Merbold, L., Metzger, S., Sedlak, P., & Siebicke, L. (2018). Estimating the storage term in eddy covariance measurements: The icos methodology. *International Agrophysics*, *32*(4), 552–567. https://doi.org/10.1515/intag-2017-0037

Montgomery, R. B. (1948). Vertical eddy flux of heat in the atmosphere. *Journal of Atmospheric Sciences*, *5*(6), 265–274. https://doi.org/10.1175/1520-0469(1948)005<0265:VEFOHI>2.0.CO;2

Myers-Smith, H., Isla, Forbes, C., Bruce, Wilmking, M., Hallinger, M., Lantz, T., Blok, D., Tape, D., Ken, Macias-Fauria, M., & Sass-Klaassen, U. (2011). Shrub expansion in tundra ecosystems: Dynamics, impacts and research priorities. *Environmental Research Letters*, *6*. https://doi.org/10.1088/1748-9326/6/4/045509

Natali, S., Watts, J., & Rogers, B. e. a. (2019). Large loss of co_2 in winter observed across the northern permafrost region. *Nat. Clim. Chang.*, *9*, 852–857. https://doi.org/https://doi.org/10.1038/s41558-019-0592-8

National Land Survey of Finland. (n.d.). *Karttapaikka map service*. Retrieved May 19, 2025, from https://asiointi.maanmittauslaitos.fi/karttapaikka/?lang=en

Obukhov, A. (1951). Charakteristiki mikrostruktury vetra v prizemnom sloje atmosfery (characteristics of the micro-structure of the wind in the surface layer of the atmosphere). *Geofiz*, 49–68.

Oechel, W. C., Laskowski, C. A., Burba, G., Gioli, B., & Kalhori, A. A. M. (2014). Annual patterns and budget of co_2 flux in an arctic tussock tundra ecosystem. *J. Geophys. Res. Biogeosci*, *119*(3), 323–339. https://doi.org/10.1002/2013JG002431

Pastorello, G., Trotta, C., & Canfora, E. e. a. (2021). The fluxnet2015 dataset and the oneflux processing pipeline for eddy covariance data. *Sci Data*, *7*. https://doi.org/https://doi.org/10.1038/s41597-020-0534-3

Peltola, O., & Mammarella, I. (2015). *Short introduction to eddyuh*. University of Helsinki, Department of Physics, Division of Atmospheric Sciences.

Rantanen, M., Karpechko, A., Lipponen, A., Nordling, K., Hyvärinen, O., Ruosteenoja, K., Vihma, T., & Laaksonen, A. (2022). The arctic has warmed nearly four times faster than the globe since 1979. *Commun Earth Environ*, *3*. https://doi.org/https://doi.org/10.1038/s43247-022-00498-3

Reynolds, O. (1895). On the dynamical theory of incompressible viscous fluids and the determination of the criterion. *Philosophical Transactions of the Royal Society of London. (A.)*, *186*, 123–164. https://doi.org/10.1098/rsta.1895.0004

Schuur, E., Abbott, B., Bowden, W., Brovkin, V., Camill, P., Canadell, J., Chanton, J., ChapinIII, F., Christensen, T., Ciais, P., Crosby, B., Czmiczik, C., Grosse, G., Harden, J., Hayes, J., Hugelius, G., Jastrow, J., Jones, J., Kleinen, T., . . . Zimov, S. (2013). Expert assessment of vulnerability of permafrost carbon to climate change. *Climatic Change*, *119*. https://doi.org/https://doi.org/10.1007/s10584-013-0730-7

Shaver, G. R., Billings, W. D., F. Stuart Chapin III, Giblin, A. E., Nadelhoffer, K. J., Oechel, W. C., & Rastetter, E. B. (1992). Global change and the carbon balance of arctic ecosystems. *BioScience*, *42*(6), 433–441. https://doi.org/10.2307/1311862

Stiegler, C., Lund, M., Christensen, R., T, Mastepanov, M., & Lindorth, A. (2016). Effects of interannual variability in snow accumulation on energy partitioning and surface

energy exchange in a high-arctic tundra ecosystem. *The Cryosphere Discuss.* https://doi.org/10.5194/tc-2016-5

Stull, B., Roland. (1988). *An introduction to boundary layer meteorology*. Kluwer Academic Publishers.

Swinbank, W. C. (1951). The measurement of vertical transfer of heat and water vapor by eddies in the lower atmosphere. *Journal of Atmospheric Sciences*, *8*(3), 135–145. https://doi.org/10.1175/1520-0469(1951)008<0135:TMOVTO>2.0.CO;2

Tennekes, H., & Lumley, L., John. (1972). *A first course in turbulence*. The MIT Press. https://doi.org/https://doi.org/10.7551/mitpress/3014.001.0001

Tybirk, K., Nilsson, M.-C., Michelsen, A., Kristensen, H. L., Shevtsova, A., Strandberg, M. T., Johansson, M., Nielsen, K. E., Riis-Nielsen, T., Strandberg, B., & Johnsen, I. (2000). Nordic empetrum dominated ecosystems: Function and susceptibility to environmental changes. *AMBIO: A Journal of the Human Environment*, *29*(2), 90–97. https://doi.org/10.1579/0044-7447-29.2.90

Watts, J., Natali, S., Potter, S., & Rogers, B. (2019). Gridded winter soil co_2 flux estimates for pan-arctic and boreal regions, 2003-2100. https://doi.org/10.3334/ORNLDAAC/1683

Webb, E. E., Schuur, E. A. G., Natali, S. M., Oken, K. L., Bracho, R., Krapek, J. P., Risk, D., & Nickerson, N. R. (2016). Increased wintertime co_2 loss as a result of sustained tundra warming. *Journal of Geophysical Research: Biogeosciences*, *121*, 249–265. https://doi.org/10.1002/2014JG002795

Weller, G., & Holmgren, B. (1974). The microclimates of the arctic tundra. *Journal of Applied Meteorology*, *13*. https://doi.org/https://doi.org/10.1175/1520-0450(1974)013%3C0854:TMOTAT%3E2.0.CO;2

Wilson, K., Goldstein, A., Falge, E., Aubinet, M., Baldocchi, D., Berbigier, P., Bernhofer, C., Ceulemans, R., Dolman, H., Field, C., Grelle, A., Ibrom, A., Law, B., Kowalski, A., Meyers, T., Moncrieff, J., Monson, R., Oechel, W., Tenhunen, J., ... Verma, S. (2002). Energy balance closure at fluxnet sites [FLUXNET 2000 Synthesis]. *Agricultural and Forest Meteorology*, *113*(1), 223–243. https://doi.org/https://doi.org/10.1016/S0168-1923(02)00109-0

Appendix A.

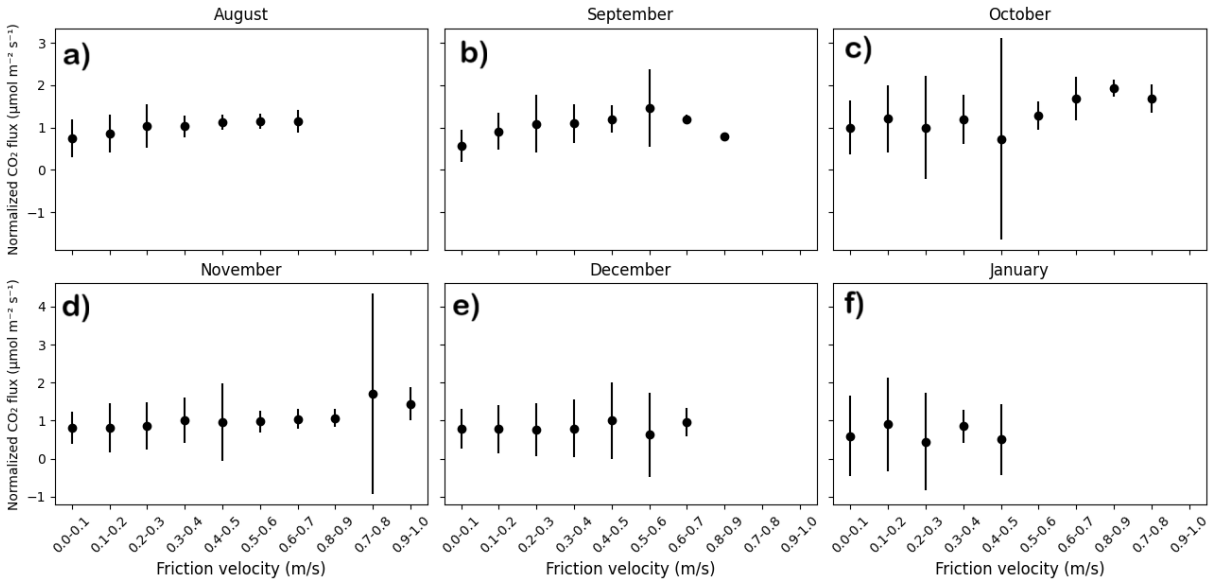

Figure A.1: Normalized nighttime CO_2 flux with respect to binned friction velocity for each month

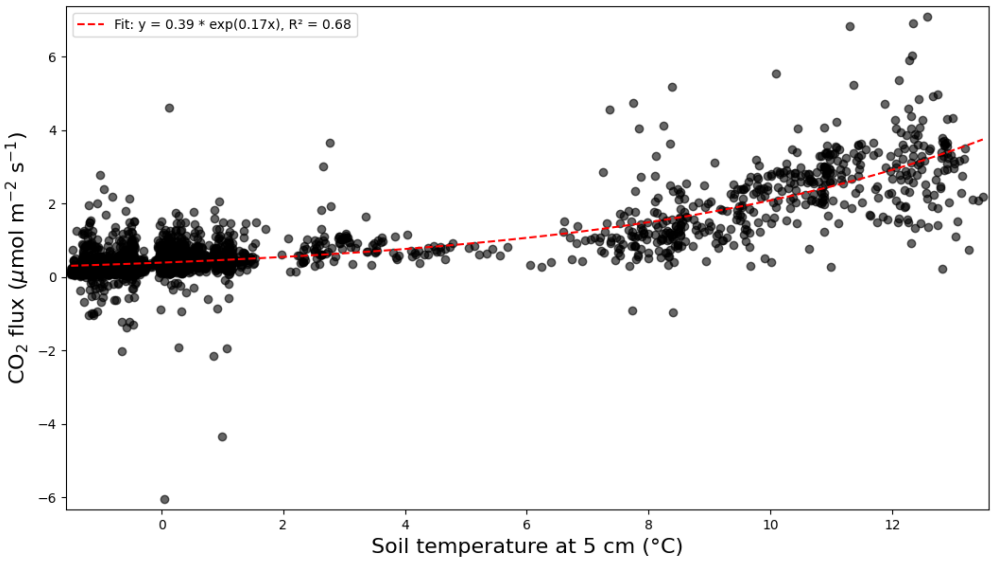

Figure A.2: Exponential fit between nighttime CO_2 flux and soil temperature